JOURNAL OF MATERIALS SCIENCE 26 (1991) 1137–1156

Particulate reinforced metal matrix composites – a review

I. A. IBRAHIM, F. A. MOHAMED, E. J. LAVERNIA
Materials Section, Department of Mechanical Engineering, University of California, Irvine, California 92717, USA

The physical and mechanical properties that can be obtained with metal matrix composites (MMCs) have made them attractive candidate materials for aerospace, automotive and numerous other applications. More recently, particulate reinforced MMCs have attracted considerable attention as a result of their relatively low costs and characteristic isotropic properties. Reinforcement materials include carbides, nitrides and oxides. In an effort to optimize the structure and properties of particulate reinforced MMCs various processing techniques have evolved over the last 20 years. The processing methods utilized to manufacture particulate reinforced MMCs can be grouped depending on the temperature of the metallic matrix during processing. Accordingly, the processes can be classified into three categories: (a) liquid phase processes, (b) solid state processes, and (c) two phase (solid–liquid) processes. Regarding physical properties, strengthening in metal matrix composites has been related to dislocations of a very high density in the matrix originating from differential thermal contraction, geometrical constraints and plastic deformation during processing.

1. Introduction

The attractive physical and mechanical properties that can be obtained with metal matrix composites (MMCs), such as high specific modulus, strength, and thermal stability have been documented extensively [1–7]. MMCs combine metallic properties (ductility and toughness) with ceramic properties (high strength and high modulus), leading to greater strength in shear and compression and higher service temperature capabilities. Interest in MMCs for aerospace, automotive and other structural applications has increased over the last five years, as a result of availability of relatively inexpensive reinforcements, and the development of various processing routes which result in reproducible microstructures and properties [8]. In aerospace applications, reductions in structural weight can be effected, not only by reducing the alloy density, but also by increasing its modulus. For example, a 50% increase in modulus, achieved by substituting a discontinuous silicon carbide reinforced aluminium alloy for an unreinforced wrought counterpart, resulted in a 10% reduction in weight [9].

Reinforcement materials include carbides (e.g., SiC, B_4C), nitrides (e.g., Si_3N_4, AlN), oxides (e.g., Al_2O_3, SiO_2), as well as elemental materials (e.g., C, Si). The reinforcements may be in the form of continuous fibres, chopped fibres, whiskers, platelets, or particulates. SiC, for example, is being used in aluminium and magnesium MMCs in all of the above mentioned forms and carbon and silicon fibres are being used in aluminium–, magnesium–, and copper–matrix composites [10].

Early studies on MMCs addressed the development and behaviour of continuous fibre reinforced high performance hybrid materials, based on aluminium and titanium matrices [11, 12]. Unfortunately, despite encouraging results, extensive industrial application of these composites has been hindered by high manufacturing costs associated with the high costs of the reinforcement fibres (i.e., \$ 660 K g^{-1} for boron fibres) and highly labour intensive manufacturing processes. As a result, utilization of these materials has been limited, almost exclusively, to military and other highly specialized applications.

The family of discontinuously reinforced MMCs include both particulates and short whiskers or fibres. More recently, this class of MMCs has attracted considerable attention as a result of: (a) availability of various types of reinforcement at competitive costs (i.e., \$4.85 K g^{-1} for SiC particulates), (b) the successful development of manufacturing processes to produce MMCs with reproducible structures and properties, and (c) the availability of standard or near standard metal working methods which can be utilized to form these MMCs [13]. Moreover, the problems associated with fabrication of continuously reinforced MMCs, such as: (a) fibre damage, (b) microstructural non-uniformity, (c) fibre to fibre contact, and (d) extensive interfacial reactions can be avoided with discontinuous reinforcements [14]. In applications not requiring extreme loading or thermal conditions, such as in automotive components, discontinuously reinforced MMCs have been demonstrated to offer essentially isotropic properties with substantial improvements in

0022–2461/91 \$03.00 + .12

strength and stiffness, relative to those available with unreinforced materials [15–18].

Although whisker reinforced MMCs have been shown to have attractive combinations of strength and thermal stability relative to those of particulate reinforced materials, extensive commercialization of whisker reinforced MMCs has been slow as a result of: (a) the high costs associated with currently available whiskers, (b) observed faulted internal structure of whiskers and irregular surface which may contain particulate contamination as observed in SiC whiskers [19], and (c) the asbestos-like health hazards associated with high aspect ratio particulates.

The family of particulate reinforced metal matrix composites include dispersion strengthened (DS) alloys and cermets. DS alloys consist of metal matrices with additions of hard insoluble particle constituents with sizes of the order of a micrometre and in small proportions, typically below 5 vol %. A cermet is a mixture of ceramics and metals. Its structure is composed of ceramic grains bonded in a metal matrix. The volume fraction of the metal matrix may be up to 30%. Bonding between metal and ceramic results from their mutual or partial solubility or from elemental additions that are partially soluble in both [20].

The objective of this work is to examine the various factors affecting: (a) processing, (b) microstructure, and (c) mechanical behaviour of discontinuously reinforced metal matrix composites. In particular, this work will address the effects of the compatibility between reinforcement and matrix, and the ensuing interfacial activity on the resulting strength and fatigue life of the MMCs, at both ambient and elevated temperatures.

2. Materials selection

2.1. Reinforcement selection

Selection criteria for the ceramic reinforcement include

(i) elastic modulus,
(ii) tensile strength,
(iii) density,
(iv) melting temperature,
(v) thermal stability,
(vi) coefficient of thermal expansion,
(vii) size and shape,
(viii) compatibility with matrix material, and
(ix) cost

Some selected properties of commonly used ceramic reinforcements are shown in Table I [10, 13, 21]. The structural efficiency of discontinuously reinforced MMCs is a function of the density, elastic modulus, and tensile strength of the reinforcing phases. The chemical stability and compatibility of the reinforcements with the matrix material are important, not only for the end application, but also during material fabrication. The thermal mismatch strain, ε, between reinforcement and matrix is an essential consideration for composites that will be exposed to thermal cycling. ε is a function of the difference between the coefficients of thermal expansion, $\Delta\alpha$, of the reinforcement and matrix according to the following expression

$$\varepsilon = \Delta\alpha\Delta T \quad (1)$$

where ΔT is the temperature change. It is important for $\Delta\alpha$ to be a minimum in order to minimize strain accumulation. It is also important to recognize that relaxation of these strains, by the formation of a dislocation network, will alter the response of the MMC to thermomechanical processing relative to that of unreinforced alloys [22, 23]. The crystal structure of the reinforcements is affected by manufacturing processes, e.g., SiC crystals may be of β (bcc) or a mixture of β and α (hcp) phases. In powder metallurgy processed MMCs, for example, the importance of selecting the appropriate SiC size to matrix powder size ratio in PM processing method has been demonstrated by ALCOA investigators [24, 25]. The results of these studies, as shown in Fig. 1 [24], indicate that there is a relationship between the toughness of SiC_p reinforced MB78 – a 7000 series aluminium alloy – and the SiC_p–Al powder size ratio. An inspection of the results shown in this figure shows that for a given volume fraction of SiC_p, toughness increases with a decrease in interparticle distance, as indicated by a higher SiC_p–Al powder size ratio.

2.2. Matrix selection

Whereas any of the commonly used structural aluminium alloys – 6xxx and 7xxx – can be utilized as matrices, the use of MMCs for elevated temperature applications necessitates the presence of thermodynamically stable dispersoids. This requirement has been achieved by using an alloy–dispersoid system in which elemental solubility, solid state diffusivity and interfacial energies are minimized, thereby minimizing coarsening and interfacial reactions [26]. For example, titanium additions to aluminium are attractive because they promote the precipitation of the Al_3Ti phase. This phase enhances the thermal stability and structural efficiency of the matrix as a result of a high melting point (1330 °C), low density (3.3 g cm^{-3}) and low diffusivity (1.69×10^{-14} cm^2 s^{-1}) in aluminium [27, 28].

The requirements of low density, with reasonably high thermal conductivity, have made aluminium and magnesium alloys the most commonly used matrices. Regarding alloying additions, the results of several studies [29, 30] have shown that low matrix alloying additions result in MMCs with attractive combinations of strength, ductility and toughness. Minor alloying elements (e.g., Mn, Cr), commonly used in wrought alloys as grain refiners, are unnecessary in discontinuous reinforced MMCs [29]. Furthermore, these additions should be avoided, since they might result in the formation of coarse intermetallic compounds during consolidation and subsequent processing, thus impairing the tensile ductility of the composite.

2.3. Matrix–ceramic interface

The interface formed between the matrix and the

TABLE I Properties of ceramic reinforcements [10, 13, 21]

Ceramic	Density ($\times 10^{-3}$ kg m^{-3})	Expansivity (10^{-6} °C^{-1})	Strength (MPa)	Elastic modulus (GPa)
Al_2O_3	3.98	7.92	221(1090 °C)	379(1090 °C)
AlN	3.26	4.84	2069(24 °C)	310(1090 °C)
BeO	3.01	7.38	24(1090 °C)	190(1090 °C)
B_4C	2.52	6.08	2759(24 °C)	448(24 °C)
C	2.18	− 1.44	–	690
CeO_2	7.13	12.42	589(24 °C)	185(24 °C)
HfC	12.20	6.66	–	317(24 °C)
MgO	3.58	11.61	41(1090 °C)	317(1090 °C)
$MoSi_2$	6.31	8.91	276(1090 °C)	276(1260 °C)
Mo_2C	8.90	5.81	–	228(24 °C)
NbC	7.60	6.84	–	338(24 °C)
Si	2.33	3.06	–	112
SiC	3.21	5.40	–	324(1090 °C)
Si_3N_4	3.18	1.44	–	207
SiO_2	2.66	< 1.08	–	73
TaC	13.90	6.46	–	366(24 °C)
$TaSi_2$	–	10.80	–	338(1260 °C)
ThO_2	9.86	9.54	193(1090 °C)	200(1090 °C)
TiB_2	4.50	8.28	–	414(1090 °C)
TiC	4.93	7.60	55(1090 °C)	269(24 °C)
UO_2	10.96	9.54	–	172(1090 °C)
VC	5.77	7.16	–	434(24 °C)
WC	15.63	5.09	–	669(24 °C)
WSi_2	9.40	9.00	–	248(1090 °C)
ZrB_2	6.09	8.28	–	503(24 °C)
ZrC	6.73	6.66	90(1090 °C)	359(24 °C)
ZrO_2	5.89	12.01	83(1090 °C)	132(1090 °C)

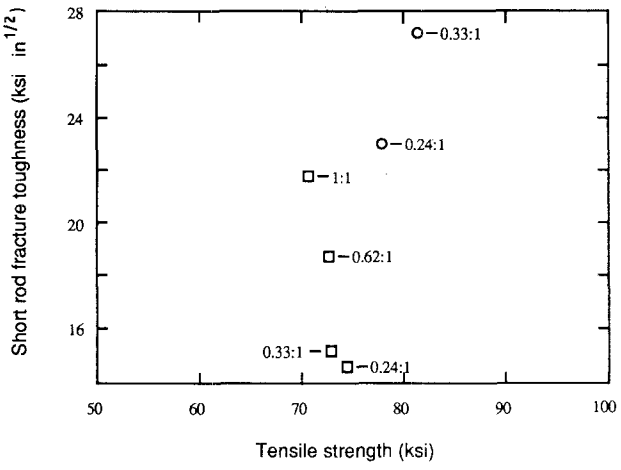

Figure 1 Influence of SiC_p–Al size ratio on fracture toughness of MB78; APD is average particle diameter [24]. (○ 15 v/o-T4, □ 20 v/o-T4.

ceramic reinforcement is of interest since the characteristics of this region determine load transfer and crack resistance of the MMCs during deformation. Systematic studies of metal–ceramic interfaces were initiated in the early 1960s [31]. It is now widely accepted that in order to maximize interfacial bond strength in MMCs, it is necessary to promote wetting, control chemical interactions, and minimize oxide formation. The interaction may be in the form of mechanical locking or chemical bonding between the matrix and the reinforcement.

Wetting is effected between a metal and a liquid when the strength of the interfacial bond exceeds the surface tension of the liquid. A measure of wettability can be obtained by measuring the contact angle, θ, see Fig. 2, formed between a solid and a liquid, as defined by Young's equation [32]

$$\gamma_{sg} = \gamma_{lg}\cos\theta + \gamma_{sl} \quad (2)$$

where γ_{sl} γ_{sg} and γ_{lg} are the interfacial energies between solid and liquid, solid and gas, and liquid and gas phases, respectively. In terms of the energetics of wetting, the work of adhesion, W_{ad}, is defined as the energy required to separate a unit area of the solid–liquid interface, according to [33]

$$W_{ad} = \gamma_{lg}(1 + \cos\theta) \quad (3)$$

Hence, wetting is achieved when $\theta < 90°$ (i.e., when $\gamma_{sg} > \gamma_{sl}$) or when the driving force for wetting, D_f, exceeds the liquid interfacial energy (i.e., $D_f > \gamma_{lg}$) [33]. The value of D_f depends on the surface tension of the liquid and the strength of the liquid–solid interface, which in turn are influenced by surface characteristics, interfacial reactions, heat of formation, valence electron concentration, temperature and time [34].

Wetting is difficult to achieve in molten metal–ceramic systems as a result of the high surface tension commonly associated with molten metals (of the order

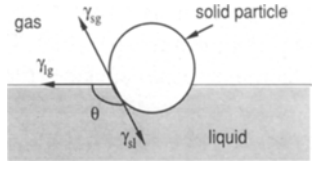

Figure 2 Schematic diagram showing contact angle formed between solid, liquid and gas phases.

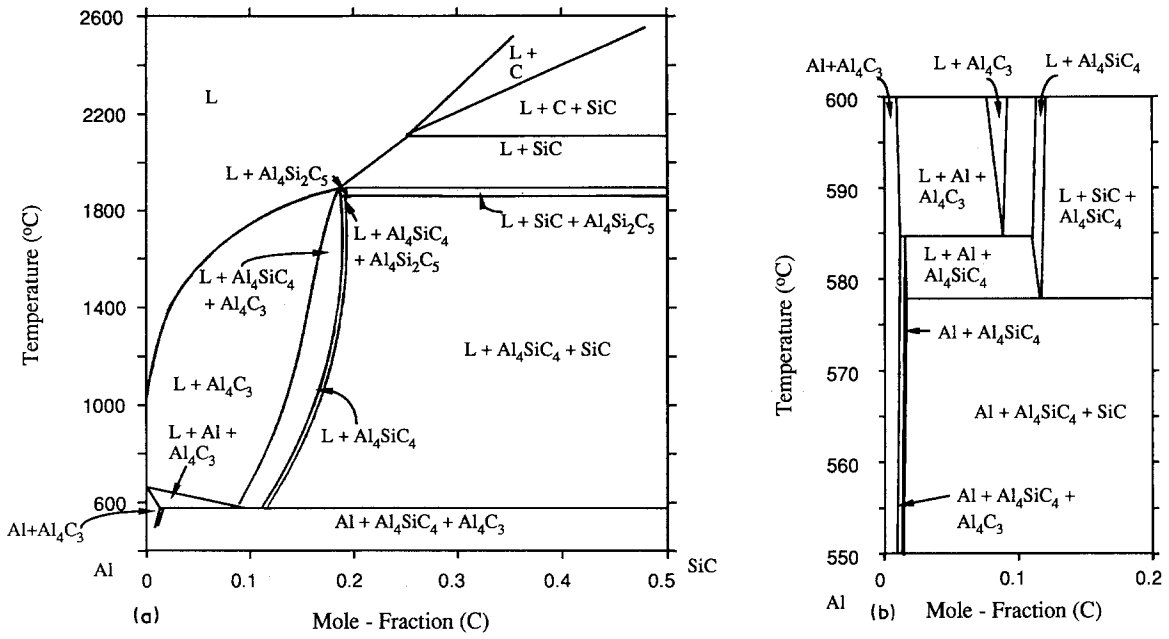

Figure 3 The Al–SiC isopleth (a) for the temperature range 400 to 2600 °C and the expanded view (b) for temperature range 550 to 600 °C [43].

of 1000 mJ m^{-2}). For example, wetting of carbon, SiC, B_4C and Al_2O_3 by aluminium and its alloys has been measured and found to be poor below 950 °C [6]. Nevertheless, wetting can be effected in these systems by promoting a decrease in the contact angle through

(1) increasing the surface energy of the solid,

(2) decreasing the solid–liquid interfacial energy, and/or

(3) decreasing the surface tension of the liquid metal.

In practice, these can be achieved by (a) applying metallic coatings to the ceramic particulates, (b) alloying the metallic matrix with reactive materials and (c) heat treating the ceramic particulates [35].

The application of metallic coatings, such as nickel and copper, to the ceramic particulates increases the overall surface energy of the particulates by altering the nature of the interface from metal–ceramic to metal–metal. Hence, wetting is achieved by effecting a strong interaction at the interface between the matrix and the reinforcement. This approach has been successfully utilized, for example, in the Al–Al_2O_3 system by coating the Al_2O_3 with nickel and Ti–Ni [36, 37].

The addition of reactive elements such as Li, Mg, Ca, Ti, Zr, and P to the matrix material improves wetting characteristics of metal–ceramic systems through: (a) a reduction of the surface tension of the melt, (b) a reduction of the solid–liquid interfacial energy of the melt, or (c) by inducing a chemical reaction at the interface. In aluminium alloys, for example, wetting of certain ceramics can be enhanced through additions of elements which have a high affinity for oxygen, such as those in group I and II, (e.g., lithium and magnesium) [38, 39]. The presence of 3 wt % Mg decreased the surface tension of pure aluminium from 0.760 to 0.620 N m^{-1}; the surface tension of magnesium is 0.599 N m^{-1} [40]. Regarding interfacial activities, chemical reactions have been observed to occur readily between Al_2O_3 and divalent transition metal oxides, resulting in the formation of aluminate spinels such as $MgO \cdot Al_2O_3$ [41]. These mineral spinels or oxides promote interfacial bonding since they form strong bonds between both metals and ceramics.

Thermal treatment of ceramic particulates has been effectively utilized to promote wetting in MMCs through desorption of adsorbed gases from the ceramic surfaces. In the presence of oxygen, metals with a high free energy of oxide formation form stable oxides which act as effective diffusion barriers that decrease the level of interaction at the interface [42]. Hence, the wettability of oxides by molten metals is poor, unless a certain temperature threshold is reached at which the oxide can be penetrated by the molten metal. In addition to thermal exposure, ultrasonic irradiation of the melt has also been shown to induce partial desorption of adsorbed gases from the ceramic particulates, thereby improving wetting. An excellent review on wetting behaviour in MMCs is available elsewhere [33].

2.3. Matrix–ceramic interaction zones

Although limited interfacial reactions may enhance the load bearing capabilities of MMCs, extensive interfacial reaction zones, exacerbated by high processing temperatures, will form to the detriment of the composite. Although some degree of wetting is necessary before interfacial reactions begin to occur, the extent and products of these reactions will depend mostly on the thermodynamic potential of the elements involved. For example, in the Al–SiC system intermediate phases such as Al_4C_3 and Al_4SiC_4 may form either as a continuous layer or isolated precipitates [43] (see Fig. 3). SiC reacts with molten Al ($T > T_m$) according to the reactions

$$4Al + 3SiC = Al_4C_3 + 3Si \quad (4)$$

$$4Al + 4SiC = Al_4SiC_4 + 3Si \quad (5)$$

Further growth occurs, in the case of the first reaction,

by solid state diffusion through the Al_4C_3 layer, and in the case of the second reaction, by the dissolution of the SiC into the liquid aluminium. Although bonding between SiC and Al_4C_3 appears to be good, the Al_4C_3–SiC interface is generally rough and can lead to regions of stress localization. For example, in the graphite–aluminium system, degradation of the graphite reinforcement also occurs by the formation and growth of Al_4C_3 at a fast rate above 550 °C. In the presence of interfacial cracks, cavities and voids, formed at the interface, new mechanisms of crack initiation and propagation, relative to the unreinforced metal, are introduced.

Quantitative and qualitative information on the presence and extent of interfacial reactions in MMCs can be obtained using various analytical techniques. In Al–SiC, for example, the presence of interfacial reactions and their associated products have been studied by

(a) Measuring the intensity of aluminium carbide and silicon X-ray peaks [44].

(b) Measuring the thickness of the ceramic–matrix interaction layer [45].

(c) Determining changes in the liquidus temperature from differential scanning calorimetry (DSC) traces [46]. This approach is based on the principle that the liquidus temperature will be depressed proportionally to the extent of silicon dissolution in the alloy.

(d) Measuring the relative intensities of silicon and aluminium across the SiC–matrix interface by scanning Auger microprobe [47].

(e) Measuring the relative concentration of silicon and aluminium across the SiC–matrix interface by scanning transmission electron microscope with X-ray energy dispersion analysis (STEM EDAX) [47].

2.4. Matrix–ceramic interface bond strength

A systematic evaluation of the interfacial bond strength in MMCs is not available, partly as a result of the numerous ceramic–matrix combinations, and partly as a result of a lack of fundamental knowledge of the interfacial characteristics of these systems. For example, direct measurements of the interfacial shear strength in MMCs have been limited to: (i) fibre pull-out tests [48] and (ii) punch tests using aluminium discs with pieces of SiC embedded in the center [31]. These approaches, however, often result in brittle fracture of the SiC. The bond strength can also be measured by applying the principles underlying the mechanism of the ductile fracture [49], provided that the ductile fracture starts by void nucleation at the ceramic particulates.

Measurement of the bond strength on the basis of ductile fracture involves establishing the local stress state during plastic deformation under a triaxial stress state [50]. A standard tensile test specimen may be used. A local triaxial stress state can be introduced by cutting a circumferential groove at the centre of the specimen, as shown in Fig. 4. The fractured specimen is sectioned parallel to the tensile axis and polished. The polished sections are then examined for voids

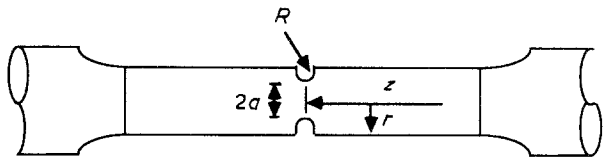

Figure 4 Tensile specimen for use in bond strength test; R, a, z, and r define the geometry of the specimen [50].

and particulate–matrix separation using the SEM. Bonding analysis [50] shows that the interfacial stress, σ_f, can be calculated from

$$\sigma_f = \sigma_T + \sigma_0 \quad (6)$$

where σ_0 is the true flow stress in tension corresponding to the local average plastic strain in the absence of the reinforcement particulates, and σ_T is the local negative pressure (the triaxial tensile stress) calculated from

$$\sigma_T/\sigma_0 = c/[1 - (r/\boldsymbol{a})^2]^{1/2} \quad z = 0 \quad (7)$$

where z is the distance along the tensile (z-) axis from the groove ($z = 0$), r the distance from the z-axis, $2a$ the diameter of the ligament, R the radius of the groove (see Fig. 4), and

$$c = 0.5\,[1 + a/R + (1 + a/R)^{1/2}]/ [2 + a/R + (1 + a/R)^{1/2}] \quad (8)$$

$$\boldsymbol{a} = a(1 + a/R)/a/R \quad (9)$$

This analysis incorporates three important assumptions: first that the volume fraction of reinforcement is small; second that the particulates are equiaxed; and third, that the material exhibits a linear strain hardening behaviour. The triaxiality, σ_T/σ_0 reaches its maximum value at the bottom of the groove ($z = 0$) where $c = 0.48$ and $\mathbf{a} = 2.3$.

The results of a study by Flom and Arsenault [3] indicate that there was no separation between the SiC particulates and the aluminium matrix. Hence, it was assumed that, for Al–SiC bond [51]

$$\sigma_f \geqslant \sigma_T^{max} + \sigma_0$$

$$\sigma_f = \sigma_0 c/[1 - (r/\boldsymbol{a})^2]^{1/2} + \sigma_0 \sim 1690\ \text{MPa} \quad (10)$$

Thus, based on this analysis, the lower bound value for the Al–SiC bond strength was estimated as 1690 MPa.

2.5. Other effects of reinforcements in the matrix

The presence of ceramic particulates has been shown to alter the ageing response of MMCs, relative to those of equivalent unreinforced materials [52–58]. Nieh and Karkac [52] and Christian and Suresh [53], for example, respectively, found that, whereas the age-hardening sequences of B_4C and SiC particulate reinforced 6061 aluminium alloy and the unreinforced alloy were similar, the kinetics of the GP zone formation and dissolution, and intermediate phase formation and precipitation, were accelerated in the

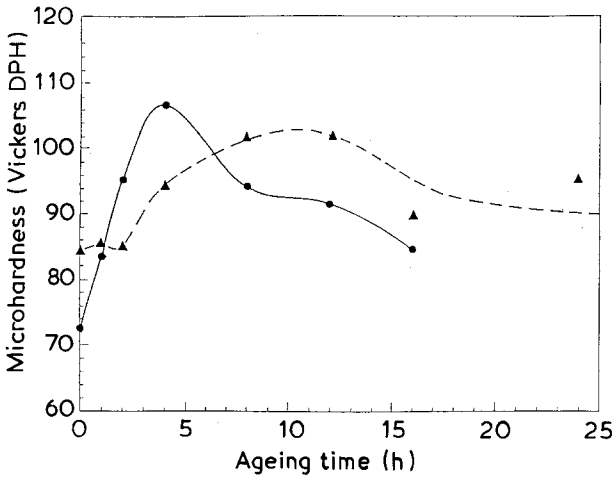

Figure 5 Artificial ageing response for unreinforced (▲) and SiCw reinforced (●) 2124 Al-alloy [53].

reinforced materials. The results of these studies show that whereas the composite reached peak hardness in 3 h at 450 °C, the equivalent hardness was attained in the unreinforced material only after 10 h (see Fig. 5).

The effects of the reinforcements, however, depend on the matrix material. For example, the presence of SiC particulates have also been shown to cause quench insensitive alloys such as Al alloy 6061 to become quench sensitive and the more quench sensitive alloys, such as Al alloy 7475, to remain unaffected [55].

The accelerated ageing and quench sensitivity commonly reported for reinforced alloys have been attributed to the presence of high diffusivity paths, such as the high density of dislocations resulting from differences in thermal expansion between the reinforcing particulates and the matrix, and to numerous heterogeneous nucleation sites causing the precipitation of GP zones or intermediate phases. The phenomenon of quench sensitivity has also been observed in PM monolithic materials but to a lesser degree [55, 56]. The nucleation sites common to both PM and MMCs are the smaller grain and subgrain sizes, oxide particles, larger dispersoids and constituent particulates [57]; in MMCs, additional nucleation sites are the high density of dislocations and the SiC–Al interfaces [56].

Regarding segregation, the work of Nutt and Carpenter [57] has shown severe segregation of magnesium and formation of MgO precipitates at Al–SiC interfaces in Al(2124)–SiC MMCs. Other phases frequently observed at Al–SiC interfaces include $CuMgAl_2$ and $CuAl_2$. The segregation of Mg, however, is not limited to MMCs. This phenomenon is well documented for monolithic Al–Mg alloys, and is generally attributed to vacancy-solute pair diffusion to boundaries due to the presence of a supersaturation of quenched vacancies [58, 59]. The depletion of magnesium and copper as well as other elements from grain interiors, will be detrimental to the behaviour of MMCs by forming local electrochemical potentials, which tends to accelerate corrosion processes. Furthermore, high concentration of these elements at the reinforcement–matrix interface will decrease the amount of elements available for age-hardening reactions.

3. Processing

A variety of processing techniques have evolved over the last two decades in an effort to optimize the structure and properties of particulate reinforced MMCs [19, 36, 60–72]. The processing methods utilized to manufacture particulate reinforced MMC can be grouped according to the temperature of the metallic matrix during processing. Accordingly, the processes can be classified into three categories: (a) liquid phase processes, (b) solid state processes, and (c) two phase (solid–liquid) processes. A critical review of the various processes follows.

3.1. Liquid phase processes

In liquid phase processes, the ceramic particulates are incorporated into a molten metallic matrix using various proprietary techniques, followed by mixing and casting of the resulting MMC. However, and as discussed in a previous section, since most ceramic materials are not wetted by the molten alloys, introduction and retention of the particulates necessitate either adding wetting agents to the melt, or coating the ceramic particulates prior to mixing.

3.1.1. Liquid metal–ceramic particulate mixing

Several approaches have been successfully utilized to introduce ceramic particulates into an alloy melt [35]. These include: (a) injection of powders entrained in an inert carrier gas into the melt using an injection gun; (b) addition of particulates into the molten stream as it fills the mould; (c) addition of particulates into the melt via a vortex introduced by mechanical agitation; (d) addition of small briquettes into the melt followed by stirring. (These briquettes are made from co-pressed aggregates of the base alloy powder and the solid particulates); (e) dispersion of the particulates in the melt by using centrifugal acceleration; (f) pushing of the particulates in the melt by using reciprocating rods; (g) injection of the particulates in the melt while the melt is being irradiated with ultrasound; and (h) zero gravity processing. The last approach involves utilizing an ultra-high vacuum and high temperatures for long periods of time.

In the processes described above, a strong bond between the matrix and the reinforcement is achieved by utilizing high processing temperatures (e.g., $T > 900$ °C for the Al–Al_2O_3 system) and alloying the matrix with an element which can interact with the reinforcement to produce a new phase and effect "wetting" between the matrix and the ceramic (e.g., Li in Al–SiC system). Agitation during processing is also essential to disrupt contamination films and adsorbed layers to facilitate interfacial bonding.

To date, liquid phase processes have reached an advanced stage of development, and SiC or Al_2O_3 (3 to 150 μm) particulates are routinely added to a

TABLE II Mechanical and physical properties of Duralcan Al–MMC alloys [61]

Alloy[a]	Yield strength (MPa)	Ultimate strength (MPa)	Elongation (%)	Modulus (GPa)	K_{IC} (MPa $m^{1/2}$)	Density ($g\,cm^{-3}$)	Electrical[b] conductivity (% IACS)	Thermal[c] conductivity ($W\,m^{-1}$)
6061–0% Al_2O_3	276	310	20.0	69	29.7			
6061–10% Al_2O_3	297	338	7.6	81	24.1			
6061–15% Al_2O_3	386	359	5.4	88	22.0			
6061–20% Al_2O_3	359	379	2.1	99	21.5			
2014–0% Al_2O_3	414	483	13.0	73	25.3			
2014–10% Al_2O_3	483	517	3.3	84	18.0			
2014–15% Al_2O_3	476	503	2.3	92	18.8			
2014–20% Al_2O_3	483	503	0.9	101	–			
A356–0% SiC	200	276	6.0	75	–	2.68	37.50	150.57
A356–10% SiC	283	303	0.6	81	–	–	–	–
A356–15% SiC	324	331	0.3	90	–	2.76	27.60	173.94
A356–20% SiC	331	352	0.4	97	–	–	–	–

[a]Solutionized to T6 condition.
[b]22 °C, F-temper.
[c]22 °C, T-temper.

variety of aluminium alloy matrices [35, 60, 61]. Among these, the DURAL process is perhaps the most advanced in terms of commercial development. The DURAL process involves the incorporation of ceramic particulates into metallic melt through melt agitation. A summary of the mechanical properties of various MMC materials processed by the DURAL process are shown in Table II. The results shown in this table suggest that it is possible to combine up to 20 vol % of either SiC or Al_2O_3 with various aluminium alloys, to obtain MMCs with attractive combinations of properties.

Despite the encouraging results obtained with liquid phase processes, some difficulties exist. These include: agglomeration of the ceramic particulates during agitation, settling of particulates, segregation of secondary phases in the metallic matrix, extensive interfacial reactions, and particulate fracture during mechanical agitation.

3.1.2. Melt infiltration

In melt infiltration processes, a molten alloy is introduced into a porous ceramic preform, utilizing either inert gas or a mechanical device as a pressurizing medium. The pressure required to combine matrix and reinforcement is a function of the friction effects due to viscosity of the molten matrix as it fills the ceramic preform. Wetting of the ceramic preform by the liquid alloy depends on: alloy composition, ceramic preform material, ceramic surface treatments, surface geometry, interfacial reactions, atmosphere, temperature and time [62–64]. This approach has been studied extensively, and in fact, is currently being used commercially to fabricate the Toyota diesel piston, an aluminium–chopped-alumina-fibre composite material [65].

Some of the drawbacks of this process include reinforcement damage, preform compression, microstructural nonuniformity, coarse grain size, contact between reinforcement fibres or particulates and undesirable interfacial reactions [19].

3.1.3. Melt oxidation processes

In melt oxidation processing (i.e., the Lanxide Process), a ceramic preform, formed into the final product shape by a fabricating technique such as pressing, injection moulding or slip casting, is continuously infiltrated by a molten alloy as it undergoes an oxidation reaction with a gas phase (most commonly air). The high temperature oxidation of the molten alloy in the interstices of the ceramic preform produces a matrix material composed of a mixture of oxidation reaction products and unreacted metal alloy [67]. The primary advantage of this process is derived from its ability to form complex, fully dense composite shapes. Attractive combinations of mechanical properties have been reported for aluminium based MMCs processed using this approach (see Table III [60]). A joint venture between Lanxide and Alcan, the Alanx Products L.P., has commercially produced a composite designated as Alan CG893, an alumina–aluminium alloy matrix grown around silicon carbide filler. This product has been demonstrated to exhibit exceptional erosive wear resistance [68].

3.2. Solid phase processes

The fabrication of particulate reinforced MMCs from blended elemental powders involves a number of steps prior to final consolidation. Two of the processes,

TABLE III Mechanical properties of some Lanxide composites [60]

Matrix–reinforcement	Four-point test (MPa)	Toughness (MPa $m^{1/2}$)
Aluminium–Al_2O_3/Al_2O_3 particulates	500	9
Aluminium–Al_2O_3/SiC particulates	523	8
Aluminium–Al_2O_3/Nicalon fibres	997	29

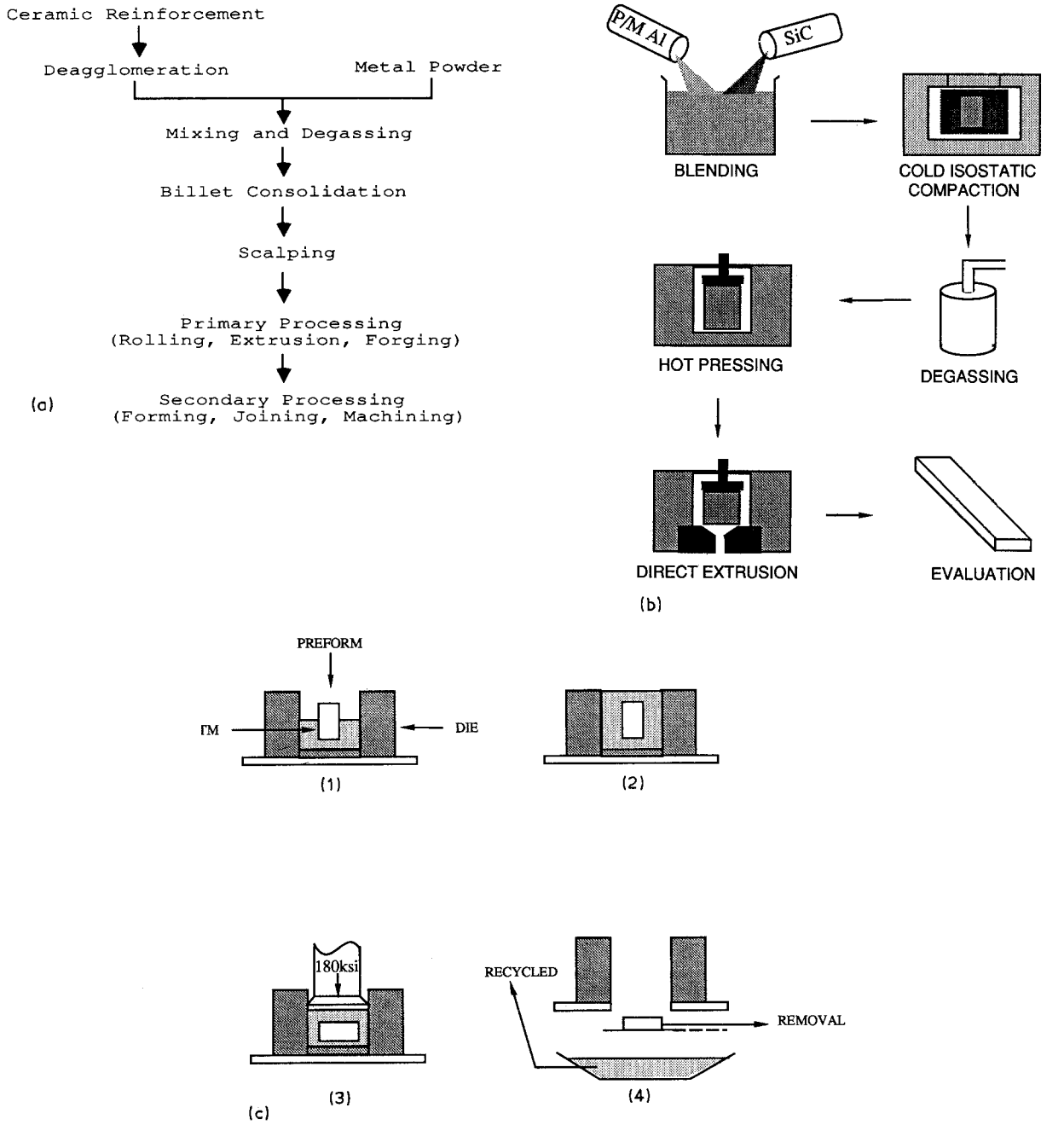

Figure 6 Schematic diagram of (a) PM–MMC fabrication steps. (b) the Alcoa process [24] and (c) the Ceracon process [66]. In the Ceracon process (1) Half of the PTM (621 °C) is poured into a preheated die, and the preform is placed into the die. (2) The die is then filled completely with the remainder of the heated PTM. (3) A pressure of 180 ksi (1.24 GPa) is applied to consolidate the preform. (4) After pressing, the part is removed, and the hot PTM is recycled to the PTM heater.

powder metallurgy and high energy rate processing are described below.

3.2.1. Powder metallurgy

Solid phase processes invariably involve the blending of rapidly solidified powders with particulates, platelets or whiskers, using a number of steps, as shown in Fig. 6a. These include: sieving of the rapidly solidified powders; blending with the reinforcement phase(s), pressing to approximately 75% density, degassing and final consolidation by extrusion, forging, rolling, or some other hot working method. This technology has been developed to various degrees of success by various commercial manufacturers, including: Alcoa (Pennsylvania, PA), Ceracon Inc. (Sacramento, CA), DWA Composites Specialities Inc. (Chatsworth, CA), Naval Surface Weapons Center, White Oak Laboratory (Silver spring, MD) and Advanced Composite Materials Corp. (Greer, SC). The Alcoa and the Ceracon processes are shown diagrammatically in Fig. 6b and c, respectively. Consolidation of the MMC preform is achieved by hot extrusion in the Alcoa process, whereas in the Ceracon process, final densification is achieved by hot pressing in a pressure transmitting medium (PTM). The PM methods have been successfully applied to a large number of metal/ceramic combinations [10, 13, 22, 24, 54, 69]. The mechanical properties of an extruded composite containing SiC whiskers and particulates are shown in Table IV [36]. The results show that PM processed Al–SiC MMCs possess higher overall strength levels relative to those

TABLE IV Typical room temperature properties of PM Al/Sic composites [69]

Material	Process	Orientation	YS (MPa)	UTS (MPa)	El. (%)	E (GPa)
6061-T6	Extrusion	–	255	290	17	70
6061-T6 (20% SiC_w)	PM/Ext	L	440	585	4	120
6061-T6 (30% SiC_w)	PM/Ext	L	570	795	2	140
6061-T6 (20%-SiC_p)	PM/Ext	L	415	498	6	97

corresponding to the equivalent material processed by a liquid phase process; the elongation values, however, are lower.

In terms of microstructural requirement, the powder metallurgy (PM) approach is superior in view of the rapid solidification experienced by the powders. This allows the development of novel matrix materials outside the compositional limits dictated by equilibrium thermodynamics [70, 71] in conventional solidification processes.

3.2.2. High-energy-high-rate processes

Another approach which has been successfully utilized to consolidate rapidly quenched powders containing a fine distribution of ceramic particulates is known as high-energy-high-rate processing [72, 73]. This approach involves the consolidation of a metal–ceramic mixture through the application of a high energy in a short period of time. An inspection of the available literature reveals that both mechanical and electrical high energy sources have been successfully utilized to consolidate MMCs [72, 73]. For example, Marcus *et al.* [73] were able to consolidate Al–SiC MMCs by heating a customized powder blend through a fast electrical discharge from a homopolar generator. The high-energy-high-rate (1 $MJ\,s^{-1}$) pulse permits the rapid heating of a conducting powder in a cold wall die. The short time at temperature approach offers the opportunity to control phase transformations and the degree of microstructural coarsening not readily possible using standard powder processing methods. This process has also been successfully applied to manufacture Al–SiC and (Ti_3Al + Nb)–SiC composites [72, 73]. Although the results are encouraging, extensive work remains to be completed in order to access the potential application of this approach. The issues that remain to be addressed include, for example, the maximum thickness that can be processed using commercially available energy sources.

3.3. Two-phase processes

3.3.1. Osprey deposition

In the Osprey process, the reinforcement particulates are introduced into the stream of molten alloy which is subsequently atomized by jets of inert gas. The sprayed mixture is collected on a substrate in the form of a reinforced metal matrix billet. This approach was introduced by ALCAN as a modification of the Osprey process [74, 75]. See Fig. 7. This process combines the blending and consolidation steps of the PM process and thus promises major savings in MMC production.

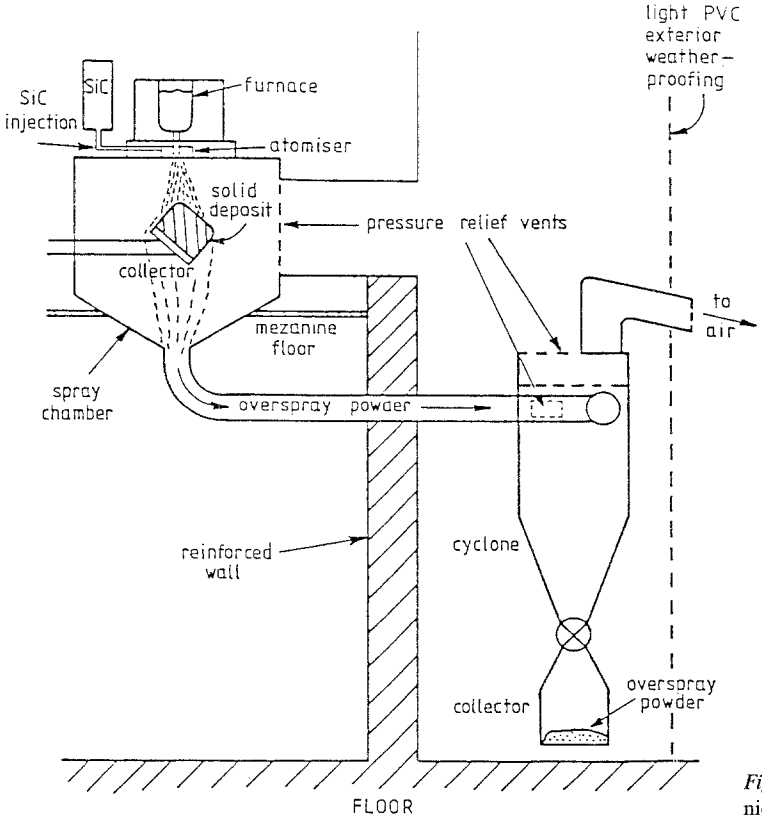

Figure 7 Schematic diagrams of modified Osprey technique [74, 75].

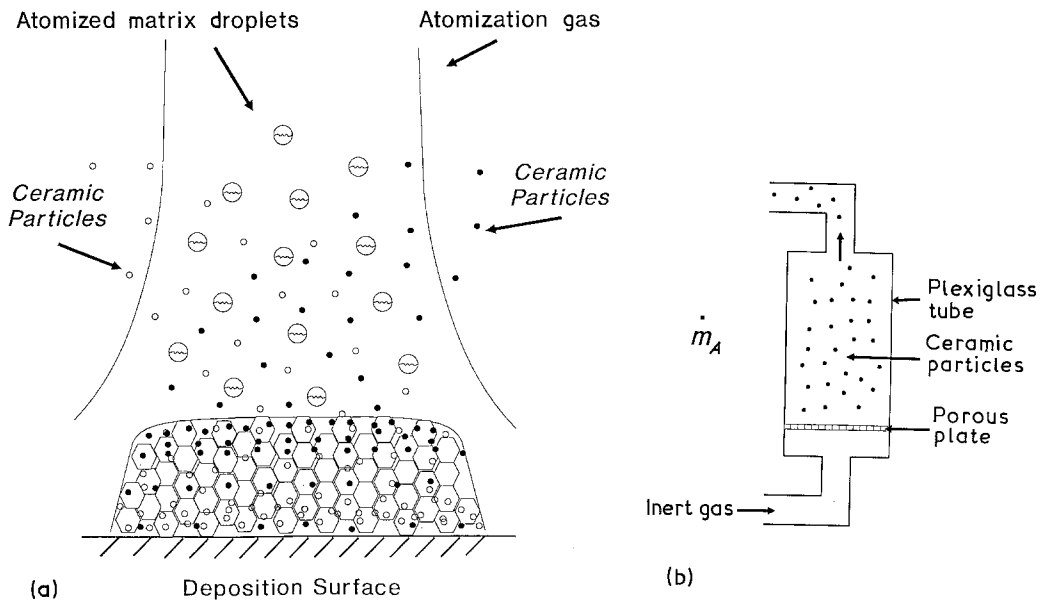

Figure 8 Schematic diagram of the variable codeposition process [78–80]. (a) gas flow, (b) fluidized bed.

3.3.2. Rheocasting

In rheocasting, the ceramic particulates are added into a metallic alloy matrix at a temperature within the solid–liquid range of the alloy, followed by vigorous agitation to form a low viscosity slurry. This approach takes advantage of the fact that many metallic alloys behave like a low viscosity slurry, when subjected to vigorous agitation during solidification. This behaviour, which has been observed for fraction solids as high as 0.5, is thought to result from the breaking of solid dendrites during stirring, into spheroidal solid particles which are then suspended in the liquid as fine grained particulates [76, 77]. This characteristic of numerous alloys, known as thixotropy, can be regained even after complete solidification by raising the temperature. This approach has been utilized in die casting of aluminium and copper base alloys [76, 77].

The slurry characteristics of the matrix during stirring permit the addition of reinforcements during solidification. The ceramic particulates are mechanically entrapped initially and are prevented from agglomeration by the presence of the primary alloy solid particles. The particulates subsequently interact with the liquid matrix to effect bonding. Furthermore, the continuous deformation and breakdown of the solid phases during agitation prevent particulate agglomeration and settling. This method has been successfully utilized by Mehrabian *et al.* [76] to incorporate up to 30 wt % of Al_2O_3, SiC, and up to 21 wt % glass particles 14 to 340 μm diameter, in a partially solidified, ~ 0.40 to 0.45 fraction solid, Al–5%Si–2%Fe alloy. The majority of the particulates were found to be homogeneously distributed in the matrix, except for coarser, 340 μm size, particulates which settled during solidification.

3.3.3. Variable co-deposition of multi-phase materials (VCM)

During VCM processing, the matrix material is disintegrated into a fine dispersion of droplets using high velocity gas jets. Simultaneously, one or more jets of strengthening phases are injected into the atomized spray at a prescribed spatial location (see Fig. 8) where the droplets contain a limited amount of volume fraction of liquid. Hence, contact time and thermal exposure of the particulates with the partially solidified matrix are minimized, and interfacial reactions can be controlled. In addition, tight control of the environment during processing minimizes oxidation [79].

In recent studies, Gupta *et al.* [78] incorporated up to 20 vol % of SiC particulates into an aluminium lithium matrix using VCM. In these studies, injection of the reinforcing phase was accomplished by entraining SiC particulates in an inert gas stream using a suitably designed fluidized bed. Fig. 9 shows a typical microstructure of an Al–Li–SiC MMC processed by the VCM method and Tables V and VI give the results of image analysis of the microstructure of five distinct experiments. The results shown in Tables V and VI indicate that the angle of injection affected the resulting distribution of SiC_p in the matrix, showing that it

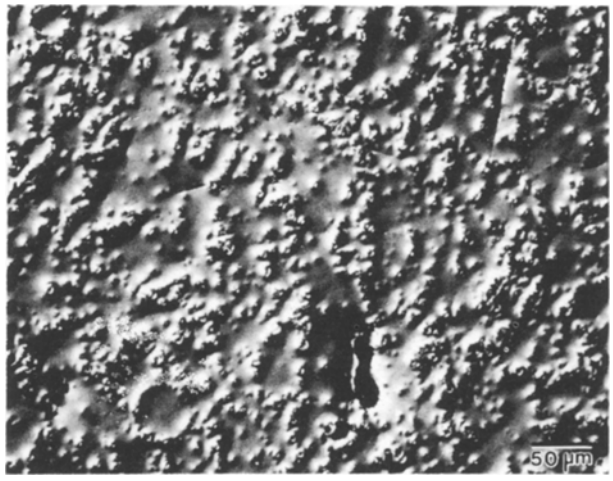

Figure 9 Structure of a VCM processed Al–Li–SiC composite [79].

TABLE V Experimental variables used in VCM study [79]

Variables	Experiment numbers				
	1	2	3	4	5
Matrix alloy	Al–Li	Al–Li	Al–Li	Al–Li	Al–Li
Reinforcement	SiC_p	SiC_p	SiC_p	SiC_p	SiC_p
Atomization pressure (MPa)	1.2	1.2	1.2	1.2	1.2
Atomization gas	Argon	Argon	Argon	Argon	Argon
Fluidized bed gas	Argon	Argon	Argon	Argon	Argon
Injection angle[a] (deg)	30	20	90[b]	30	30
Fluidizing pressure (MPa)	0.69	0.69	0.69	0.69	0.69
Flight distance (m)	0.41	0.41	0.41	0.41	0.41
Pouring temperature (°C)	840	840	840	840	840
Metal delivery tube diameter (mm)	3.30	3.27	3.33	3.05	3.00
Atomization nozzle pressure condition (kPa)[c]	~0	6.0	~0	~0	~0

[a] The injection angle refers to the relative angle between the spray of SiC_p and the concentric vertical axis of the atomized matrix.
[b] The 90° injection was conducted at a matrix flight distance of 0.15 m.
[c] Positive and zero values represent pressurization and metal free-fall respectively.

TABLE VI Results of image analysis of Al–Li–SiC_p composite [79]

Sample[a]	Equivalent diameter (μm)[b]				Volume fraction (%)				Particle spacing (λ, μm)
	Min.	Max.	Mean	σ	Min.	Max.	Mean	σ	
1A	0.57	09.00	2.70	2.01	1.92	08.33	3.49	1.82	14.48
1B	0.57	10.00	2.71	2.10	2.89	06.15	4.56	1.13	12.69
1C	0.57	12.00	2.10	1.76	4.40	13.44	7.89	1912	07.48
2A			not determined		–	9.60	08.71[d]		
2C			not determined		–	11.65[c]	07.91[d]		
3A	0.57	11.00	2.76	2.13	4.69	7.19	6.12	0.85	11.14
3B	0.57	10.00	2.86	2.12	4.38	6.10	5.13	0.50	12.62
3C	0.57	9.00	3.34	2.16	1.34	3.16	2.49	0.54	21.16
4A	0.25	13.56	1.65	2.92	18.39	24.72	20.75	2.25	18.14
4B	0.25	9.33	1.54	2.34	3.17	07.36	05.41	1.56	25.71
5A	0.25	10.68	1.61	2.79	2.60	07.63	03.70	1.54	19.99
5B	0.25	16.95	2.27	4.24	2.77	08.95	06.00	2.29	11.89
5C	0.25	18.92	2.58	4.83	0.76	15.00	05.29	5.23	10.78

[a] A, B, C designations refer to top, centre and bottom regions, respectively, of the spray deposited Al–Li–SiC_p.
[b] The equivalent diameter is a measure of the size of the SiC particulates.
[c] These values of the volume fraction were determined using quantitative metallography.
[d] These values were computed for a SiC_p size of 2.7 μm.

is possible to tailor the resulting variations in volume fraction of SiC_p through changes in injection angle. The higher volume fraction of SiC_p observed in experiment 2 was thought to be the result of the pressurization condition at the metal delivery tube (see Table V). This condition, which is caused by the relative position of the metal delivery tube and the gas jets, reduces the flow rate of the matrix, effectively decreasing the Al–Li–SiC_p mass flow ratio, hence resulting in higher SiC_p concentration [79]. Regarding the size distribution of the SiC_p, the results from Tables V and VI (d_{50} = 2.7 μm) were found to be consistent with the initial SiC_p size (d_{50} = 3.0 μm) used in this study. The slight reduction in particulate size is attributed to the difficulties associated with fluidizing the coarse SiC particulates [79].

4. Physical and mechanical properties

Particulate reinforced MMCs offer significant opportunities for developing structural materials possessing combinations of physical and mechanical properties which are not achievable with monolithic alloys. The wide selection of matrices and reinforcements permits the development of MMCs with low density, coefficient of thermal expansion (CTE) with concomittant increases in elastic modulus and thermal conductivity (TC).

Although particulate reinforced MMCs exhibit attractive mechanical properties, such as high tensile strength, creep and fatigue resistance, less than optimum ductility and fracture behaviour have limited widespread usage of these materials. In the next section, the physical and mechanical properties of

particulate reinforced MMCs are reviewed, with emphasis on strengthening mechanisms and predictive correlations. This is subsequently followed with a discussion of the behaviour of MMCs at ambient temperatures, with emphasis on cyclic deformation. Finally, this section closes with a discussion on elevated temperature behaviour and deformation mechanisms.

4.1. Physical properties

Low density MMCs can readily be developed by selecting low density alloys, such as those based on Al and Mg, for the matrix material. When structural requirements demand optimal strength–density ratio in combination with thermal stability, nickel and titanium base alloys can also be selected. Whereas most metallic matrices exhibit reasonably high thermal conductivities (TC), their CTEs are substantially higher than of most of the reinforcements available (see Table I). For example, since a number of oxide and carbide reinforcements exhibit CTEs of nearly zero, these could be utilized in high volume fractions ($V_f \sim 40\%$) to produce MMCs which exhibit extremely low CTEs.

Regarding the prediction of properties of MMCs from the properties of the individual components, numerous mathematical models have been formulated. The simplest model commonly used is the rule-of-mixture (ROM) approximation, in which the CTE, density, strength, modulus or any other desired property of the MMC can be computed from the weighted average of the individual components:

$$\alpha_c = \alpha_m V_m + \alpha_r V_r \quad (11)$$

where α is the property of interest, V the volume fraction and the subscripts c, m and r refer to the composite, matrix and reinforcement, respectively. Limitations to the ROM approximation have resulted in correlations which take into account, for example, the non-isotropic properties of high aspect ratio reinforcements and the effects of thermal barriers at the interfaces. Considering the effects of isostatic stress, Turner [10, 81] proposed that the CTE of the composite can be computed from:

$$CTE_c = (CTE_m V_m K_m + CTE_r V_r K_r)/(V_m K_m + V_r K_r) \quad (12)$$

where K is the bulk modulus of the phase. The CTE predicted by this model is significantly lower than that predicted by the ROM approximation. Kener [82] proposed a more complicated model which takes into account the effects of shear stresses between matrix and isotropic, approximately spherical, reinforcements:

$$CTE_c = CTE_m - V_r(CTE_m - CTE_r)\cdot A/B \quad (13)$$

where

$$A = K_m(3K_r + 4\mu_m)^2 + (K_r - K_m) \times (16\mu_m^2 + 12\,\mu_m K_r)$$

$$B = (3K_r + 4\mu_m)[4V_r\,\mu_m(K_r - K_m) + 3K_m K_r + 4\,\mu_m K_r]$$

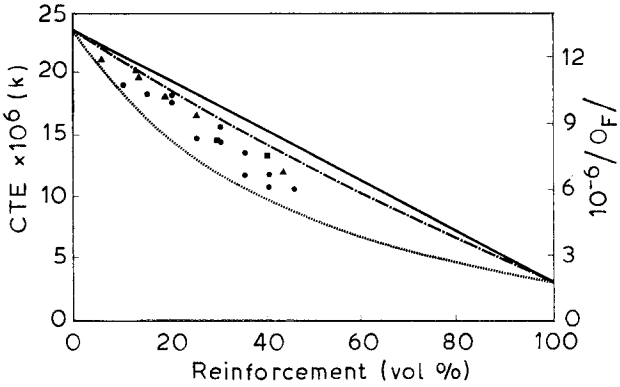

Figure 10 The measured CTE values of Al and Mg matrix composites reinforced with SiC (●), B_4C (▲), or AlN (■) and CTE values predicted by Kerner and Turner models [10]. (———) ROM, (—·—) Kerner, (- - - - -) Turner.

where μ is the shear modulus. The predictions of this model fall between those computed from the ROM and those computed using the Turner model. The measured CTE values of aluminium and magnesium matrix composites reinforced with SiC, B_4C, or AlN all fall between the values predicted by Kerner and Turner models as shown in Fig. 10, indicating that these thermoelastic models provide reasonably accurate CTE predictions.

The TC of a composite can be estimated from the model originally proposed by Rayleigh [83]:

$$k_c = k_m[(1 + 2V_r)(1 - k_m/k_r)/(2k_m/k_r + 1)]/[(1 - V_r)(1 - k_m/k_r)/(k_m/k_r + 1)] \quad (14)$$

where k is the thermal conductivity. The effects of thermal barriers due to the matrix–reinforcement interface is, however, not taken into consideration in Equation 14.

The elastic modulus of a composite can be estimated from the model proposed by Hashim and Shtrikman [84].

$$E_c = E_m[E_m V_r + E_r(V_r + 1)]/[E_r V_m + E_m(V_r + 1)] \quad (15)$$

where E is Young's modulus: the remaining terms have been defined previously. The predictions obtained utilizing Equations 14 and 15 are in good agreement with experimental values, and hence can be used to estimate the properties of composite materials.

The modulus of elasticity of MMCs is primarily affected by reinforcement content, in agreement with equation [15]. In 6061 Al matrix composites, for example, the elastic modulus has been reported to increase with reinforcement content, but is found to be independent of the type of reinforcement [85]. Heat treatment may have a slight effect on modulus of the composites; the T6-temper condition was found to exhibit a lower modulus relative to that of the as fabricated F-temper [85].

4.2. Strengthening mechanisms

The strength of a crystalline solid is determined by the stress required to either generate or move dislocations

across a span of the lattice. The latter is a more important factor in two-phase alloys (matrix plus a divided second phase). Dislocation motion is controlled either by the dislocation–dislocation interactions, direct dislocation–particulates interaction or by dislocation interaction with some matrix structure defined by the presence of dispersoids (indirect dislocation–particulates interaction).

The strengthening mechanisms in metal matrix composites have been related to a high dislocation density in the matrix originating from differential thermal contraction [86], geometrical constraints [87] and plastic deformation during processing.

The generation of dislocations as a result of differential thermal contraction is caused by the large difference in coefficient of thermal expansion (CTE) of the matrix and the ceramic reinforcement. The misfit strains occurring at the matrix–ceramic interface from thermal contraction during cooling are sufficient to generate slip dislocations. The CTE of aluminium, for instance, is ten times larger than that of SiC. Hence, a misfit strain, ε, of about 1% is developed in the aluminium matrix at the circumference of a 1 μm diameter SiC particulate. This results in a dislocation density, ρ, of $1.8 \times 10^{13}\,m^{-2}$, calculated using $\varepsilon = \rho L b$, where $L(=1\ \mu m)$ is interparticle spacing and b is the Burgers vector of aluminium. These dislocations form what is commonly known as a dislocation induced substructure.

The presence of geometrical constraints also generates additional dislocations in the matrix. For example, during deformation of a ductile matrix containing a dispersion of hard particulates, continued plastic flow necessitates the formation of dislocations in order to avoid void formation. The density of geometrically necessary dislocations, ρ, is given [87] by

$$\rho = 4\gamma/\lambda b \tag{16}$$

where λ is the geometrical slip distance, γ is the shear strain.

From the work of Vogelsang *et al.* [88], the intensity of dislocation generated at the Al–SiC interface is increased by increasing the size and shape complexity of the SiC particulate. Furthermore, Lee *et al.* [89] predicted that as the particulate size or particulate surface curvature increases, the plastic zone size also increases.

Plastic deformation during processing introduces dislocations which might form substructures that could control the flow stress of the metal–ceramic material. These dislocations may be immobilized by the ceramic particulates and thus be retained in the matrix after annealing.

Different models describing strengthening mechanisms in two-phase alloys have been reviewed by Ansell [90]. Plastic deformation resulting from extensive dislocation motion would occur if the moving dislocations could circumvent the dispersed phases by some bypass mechanism. The flow stress would, therefore, be controlled by the stress required to operate this bypass mechanism. The two bypass mechanisms proposed for low temperature deformation ($< 0.5\ T_m$) are dislocation bowing, as proposed by Orowan [91] and cross-slip as proposed by Ashby [92]. In the former case the yield stress of a material containing a dispersion of hard phases can be represented by the expression

$$\sigma_s = \tau_s + \omega \mu_M b/L \tag{17}$$

where $\omega = 1/2[1 + (1 + \upsilon)^{-1}] \ln(L/2b)$, τ_s, μ_M, b, υ, are the resolved flow stress, the shear modulus, the Burgers vector and the Poisson's number of the matrix, respectively, and L is the diameter of a semicircular dislocation. The formulation of Equation 17 assumes that the dislocations be confined to their slip planes and that the particulates are unshearable. The Ashby cross-slip mechanism involves dislocations bypassing the particulates by double cross slipping on to another slip plane.

Other mechanisms contributing to strengthening include the forest interaction of slip dislocations with the matrix dislocations, as proposed by Guyot [93]; the interaction between the matrix dislocations and the CTE induced dislocation substructure as proposed by Dew-Hughes [95]; and the interaction between the dislocation and the boundary network of dispersion stabilized subgrain boundaries as proposed by Fisher *et al.* [96].

Extensive plastic deformation will occur in two-phase alloys in which dislocations cut through or shear the second phase particulates. The plastic strain resulting from particle bypass by Orowan bowing is of the order of 10^{-4}. The Orowan model is, therefore, descriptive of microyielding rather than gross yielding of a two-phase alloy [97]. Particle shear is, thus, required for the gross yielding to occur. The matrix dislocation mobility and hence the flow stress of the matrix is controlled by the resistance of the particulate to shear. The energy, U_r, required to move a dislocation in the crystal lattice by a resolved shear stress, τ, is

$$U_r = \tau b A \tag{18}$$

where A is the area on the slip plane traversed by the dislocation. In order to cause yielding, the shear stress due either to the dislocation piled-up against or around the particle must shear the particles. The energy required to cause particle shear is a function of the structure of the matrix and second phase and their mutual orientation in space. For coherent particles, shearing will occur by the passage of matrix dislocations through the particles. Particle deformation directly follows bulk alloy strain and according to Kelly and Nicholson [98], U_r equals the energy required to cause particle shear and is a function of the structural changes such as: (a) increase of particle–matrix interface area, (b) anti-phase boundary formation if the dispersed phase is ordered, and (c) dislocation dipole formation and extension. The fracture stress of coherent phases, F, is, therefore

$$F = (\gamma_s^n/d_i + \gamma_B/b + \mu b/2d_i)\cos^2\psi \tag{19}$$

where d_i is the mean particle intercept diameter on the slip plane and ψ is the angle between the primary and cross slip planes.

For incoherent particles [97, 99], the particle-matrix interface is equivalent to a grain boundary and so precludes the passage of a dislocation. Particle shear will occur if the resolved shear stress, induced by the dislocation array against the particle, causes dislocation motion within the particles. Slip must take place in several slip systems of the second phase in order to satisfy the strain compatibility required between the two phases. Since this is difficult, relaxive matrix dislocation motion near the particle is required. The particle–matrix interface may fail causing void formation, and therefore, a significant amount of particle shear may not be expected. When particle shear occurs the shear stress, τ_p, on the particle due to a dislocation pile-up, is

$$\tau_p = n\tau = 2\lambda\tau^2/\mu_M b \quad \text{for } r > \mu_M b/\tau \quad (20)$$

$$\tau_p = n\mu_M b/r = 4\lambda\tau/d_i \quad \text{for } r < \mu_M b/\tau \quad (21)$$

where $n = (2\lambda\tau/\mu_M b)$ is the number of dislocations in the pile-up and τ is the externally applied resolved shear stress on the crystal, μ_M is the shear modulus of the matrix, r the radius of curvature of the dislocation nearest the particle, and λ the interparticle spacing. The shear stress, F, for the particle is, generally, proportional to its shear modulus, μ_p. The flow stress is, therefore

$$\sigma = (\mu_M\mu_p b/2\lambda C)^{1/2} \quad \text{coarse particles} \quad (22)$$

$$\sigma = \mu_p r/2\lambda C = \mu_p d_i/4\lambda C \quad \text{fine particles} \quad (23)$$

where C is a constant (equal to 30 for defect free particles and 1000 for defective particles). λ can be calculated from $(\lambda + d = 0.806/f^{1/3})$.

4.3. Ambient temperature behaviour

4.3.1. Tensile properties

There are numerous factors influencing the yield (YS) and tensile (TS) strength of particulate reinforced MMCs. These factors are complex and interrelated. For example, one of the most important factors influencing the mechanical behaviour of MMCs is the alloy matrix. Whereas alloys exhibiting relatively high YS and TS levels result in MMCs with concomittant increases in strength, their deformation behaviour is typically extremely poor. Furthermore, heat treatment affects the transition from elastic to plastic behaviour; hence, peak aged MMCs (i.e., T6-temper) exhibit a slightly greater amount of elastic strain, YS and TS values than those in the as fabricated condition (F-temper) [85]. This increase in the flow stress of the composites with heat treatment is likely to be an indication of the additive effects of dislocation interaction with both the alloy precipitates and the reinforcements [85]. Although increasing the volume fraction of reinforcements generally increases the strength of the MMCs, the magnitude of the increase depends, among other factors, on the volume fraction of reinforcement. In the Al–SiC_p system, for instance, the rate of increase in strength with volume fraction decreases beyond approximately 30 to 40 vol % SiC. Fracture of the MMCs containing this amount of reinforcement typically occur while still in the steeply ascending portion of the stress–strain curve [85]. (See Fig. 11.)

The mechanical properties of MMCs are also affected by the residual stresses which form as a result of the differences in the thermal expansion coefficients between the matrix and reinforcement. There are various models which have been developed to estimate the residual stresses in MMCs. For instance, the models developed by Eshelby [100], Mura and Taya [101], and Tanaka and Mori [102] can be utilized to predict the yield stress, both in tension as well as compression.

Analysis of the theoretical model proposed by Eshelby [100], in combination with the X-ray diffractometry studies conducted by Arsenault and Taya [103], reveal some interesting trends. First, the theoretical model predicts a yield stress which is higher in compression than in tension; this is in agreement with experimental results. Second, the predicted values of the yield stress of the MMCs were found to be less than those experimentally determined both in tension and compression. This discrepancy was attributed to the high dislocation density present in the annealed MMCs, and which is not considered in the development of the models. Third, although the average residual stress in the MMCs is relatively small, there can be relatively substantial compressive stresses at the matrix–reinforcement interface. In addition, the state of stress in the matrix region adjacent to the reinforcements may be either tensile or compressive, depending on the size, distribution and loading of the strengthening phases. Fourth, in the matrix region between the reinforcements, the residual stress will be tensile, and plastic deformation is likely to initiate in this since it contains fewer dislocations when compared to the reinforcement–matrix interface.

Regarding deformation and fracture mechanisms in particulate reinforced MMCs, however, our knowledge is still limited. For example, the critical factors affecting the dependence of fracture toughness on the size and distribution of strengthening phases have yet to be established. Whereas from the aforementioned discussion on melting and interfacial reactions it is clear that some sort of bond will be necessary in order to accomplish efficient load transfer, it is not obvious whether a strong or a weak bond is preferable. For example, during dynamic deformation, and as will be discussed in a subsequent section, a weak interface can effectively promote crack arrest during fatigue crack propagation. In addition, fracture of the strengthening particulates [16, 104] as well as matrix fracture [16, 105, 106] have been reported to control the deformation of particulate reinforced MMCs.

4.3.2. Fatigue properties

The lack of systematic studies, addressing the role of composite microstructure in controlling fracture [15, 107–110] and fatigue resistance [111–118] in MMC materials, has contributed to our current limited understanding of deformation and fracture in particulate reinforced MMCs. Shang *et al.* [119] investigated the

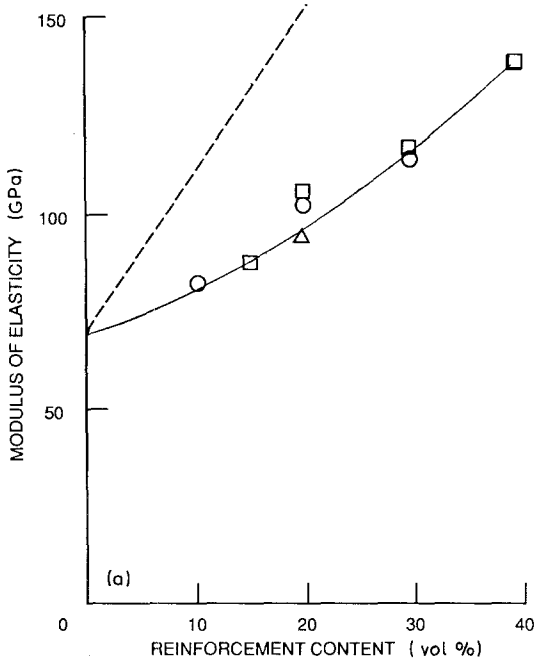

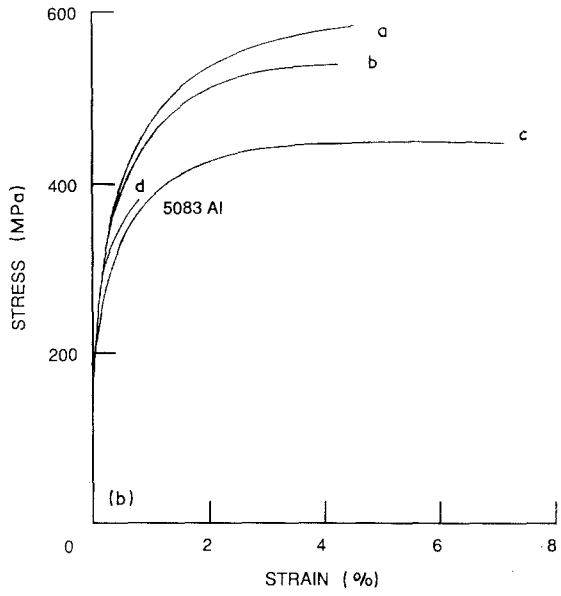

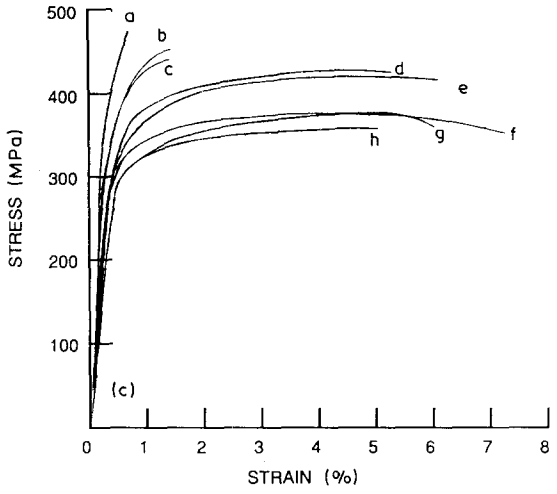

Figure 11 (a) Effect of reinforcement content (○ SiC_w (whisker), △ SiC_n (nodule), □ SiC_p (particulate), ——— isostrain-type behaviour) on modulus of elasticity of discontinuous SiC/6061 Al composites, (b) effect of Al matrix alloy an stress–strain behaviour of composites with 20 vol % SiC_w reinforcement (a 7075 Al, b 2124 Al, c 6061 Al, d 5083 Al), (c) Stress–strain curves of -6 temper SiC/6061 Al composites [85]. (a 40 vol % SiC_p, b 30 vol % SiC_w, c 30 vol % SiC_p, d 20 vol % SiC_p, e 20 vol % SiC_w, f 10 vol % SiC_w, g 20 vol % SiC_n, h 15 vol % SiC_p).

primary mechanisms governing the role of the particulates in influencing fatigue crack propagation in PM Al–SiC particulates (20 vol %) at $R = 0.1$. It was observed that fatigue crack performance, with either fine (nominal size 5 μm) or coarse (nominal size 16 μm) SiC particulates, relative to that of the unreinforced alloy, depends critically on the interaction between cyclic crack growth in the softer matrix and the decohesion, or more importantly brittle fracture, of the harder particulates. This interaction varies with the stress intensity levels (ΔK) and the size distribution of the particulates. At low ΔK levels, the fatigue crack path showed some tendency to avoid the particulates, while at higher ΔK levels particulates have less of an influence on the crack path. The amount of SiC particulate fractured during deformation increased by an order of 5 as ΔK increased. In this study, an increase in fatigue crack growth rate at low ΔK (near threshold) was observed for the MMCs containing fine (5 μm) SiC particulates, relative to the unreinforced material and to the MMC material containing coarse SiC (16 μm) particulates (see Fig. 12). This observation was attributed to the lower levels of crack closure associated with the fine SiC particulates relative to the coarse ones. Furthermore, the growth rates were observed to become progressively lower at higher ΔKs, as a result of the mutual competition of particulate fracture ahead of the crack tip (which enhances crack growth), and crack bridging from the resulting ligaments behind the crack tip (which retards the crack growth). At high ΔKs approaching instability (K_{IC}), growth rates were generally higher in both fine and coarse particulate MMCs compared to unreinforced alloy, due to their much lower fracture toughness values.

4.3.3. Fatigue crack growth mechanisms

The mechanisms of bridging induced by uncracked ligaments behind the crack tip was deduced from studies on Al–SiC_p system [117], as discussed in the previous section. Such ligaments, although not continuous in three dimensions, act in any one two-dimensional section to inhibit crack opening. This mechanism, also observed in monolithic materials [113–117], appears to result from fracture events triggered ahead of the crack tip or from general non-uniform or discontinuous advance of the crack front. In Al–SiC_p systems, for example, it predominates at intermediate fatigue crack growth rates (10^{-9} to 10^{-6} m cycle^{-1}) where cleavage of SiC particulates ahead of the crack tip becomes significant [119].

There are two types of ligament bridging which have been reported during fatigue propagation at intermediate stress intensities in Al–SiC_p composites.

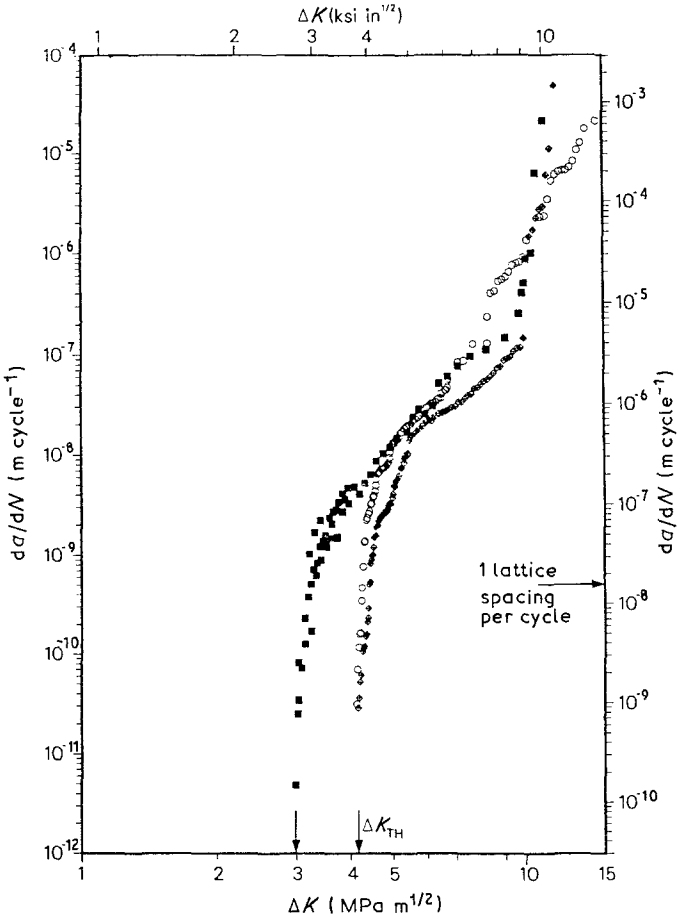

Figure 12 Variation in fatigue crack propagation rates (da/dN) with nominal stress-intensity range (ΔK) at $R = 0.1$ for the fine (5 μm) (■) and coarse (16 μm) (◇) SiC_p–Al composites and unreinforced (○) matrix alloy in the peak-aged condition [119].

In alloys with high SiC volume fractions (greater than 20 vol %), the uncracked ligaments are predominantly coplanar with the crack and are reportedly associated with fracture of carbides ahead of the crack tip; however, it has a small effect on crack-growth rates [119–121]. In alloys with lower SiC volume fractions, the ligaments are principally formed by overlapping cracks on different planes and the effect on growth rates is considerably large. The former is controlled by crack opening. In view of these results, a limiting crack-opening displacement model was proposed to describe the degree of crack-tip shielding [120]. The latter is limited by the strength of the ligament and is thus described by the limiting strain model.

The basis of the limited crack-opening displacement model is that the stress in any ligament behind the crack tip is related to the crack opening at that point; specifically the displacement in the last unbroken ligament at the end of the bridging zone must approach the limiting crack-opening displacement for fracture of the ligament. In the case of the limiting strain model, the bridges are represented as tensile ligaments, where the stress in a ligament is proportional to the strain [121].

4.4. Elevated temperature behaviour

The use of particulate reinforced MMCs for high temperature applications requires a fundamental knowledge of the mechanisms affecting their creep behaviour. Unfortunately, creep studies of particulate reinforced MMCs have been limited. Some of the available results are shown in Figs 13 to 15. At relatively low volume fractions (less than 20 vol %), the particulate reinforced MMC shows virtually no primary or secondary creep behaviour but is characterized by a progressively increasing creep rate over most of the creep life [122]. At higher volume fractions (greater than 20 vol %), however, primary, secondary, and tertiary stages were observed by several investigators [123–127]. Creep studies of whisker reinforced MMCs [123, 125] and particulate reinforced MMCs [126] report a high stress exponent and a high activation energy, similar to that reported for oxide dispersion strengthened alloys (ODS) and precipitation strengthened alloys (e.g., nickel-base superalloys and Al–Li alloys) where the dispersoids act as obstacles to dislocation motion [127]. The creep behaviour of particulate MMCs had been described by an empirical

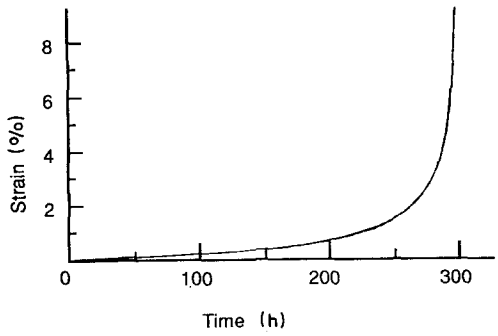

Figure 13 Creep curve for 13 vol % SiC_p–2014 Al at 473 K [122]. T = 473 K; σ = 150 MPa.

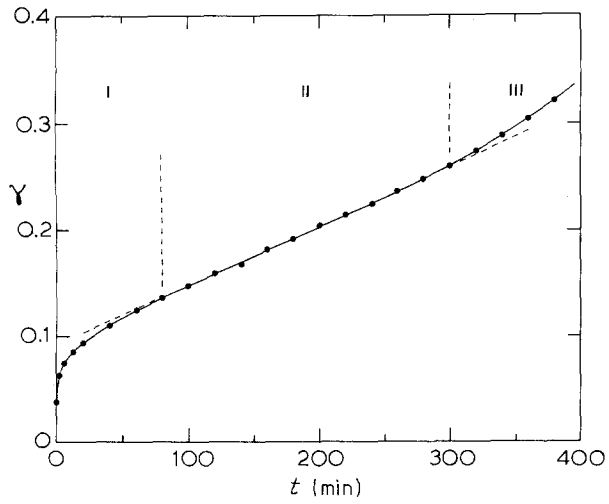

Figure 14 Creep curve for 30 vol % SiC_p–6061 Al at 648 K, ↑ = 14.1 MPa, and $\dot{\gamma}_s = 9 \times 10^{-6}\ s^{-1}$ [126]. (Region I $d\dot{\gamma}/dt < 0$, Region II $d\dot{\gamma}/dt = 0$, Region III $d\dot{\gamma}/dt > 0$).

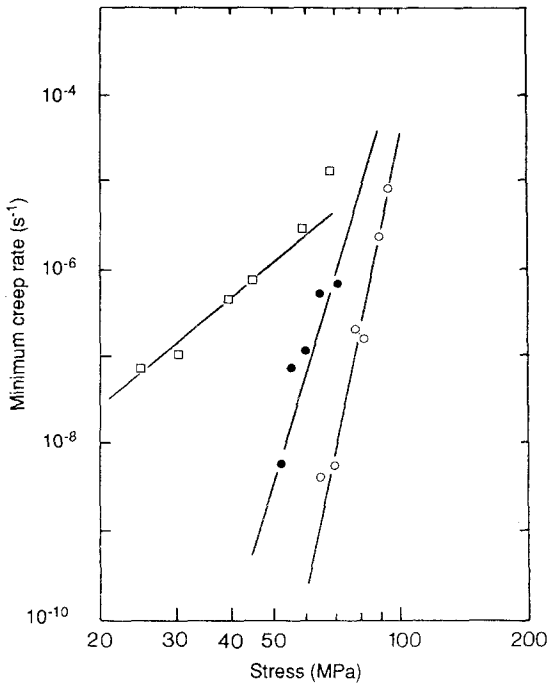

Figure 15 Minimum creep rate as a function of stress for unreinforced (□), 20 vol % SiC_p reinforced (○) and 20 vol % SiC_w reinforced (●) 6061 Al matrix alloy [123].

equation of the type [125]

$$\gamma'_{min}(sec^{-1}) = A\tau^n exp(-Q/RT) \quad (24)$$

where γ'_{min} is the minimum creep rate, A a constant that depends on structure and temperature, τ the applied shear stress, n the stress exponent, Q the activation energy; for example, $n = 9.5$ and $Q = 400\ kJ\ mol^{-1}$ for a 20 vol % 2124 Al–SiC_p system. However, an important feature of ODS alloys, i.e., a threshold stress, has not been observed in the MMCs. In a study by Divecha *et al.* [15], a particulate reinforced MMC (similar to Al–Li–SiC_w) was found to be stronger relative to the unreinforced alloy at low creep rates, but weaker at high creep rates ($\gamma' > 10^{-4}\ sec^{-1}$). This behaviour was thought to result from the reinforcements being too coarse to act as effective barriers to dislocation motion at high temperatures.

It was reported that under the same test conditions the particulate reinforced composite can be as much as 100 times less creep resistant than that of the whisker reinforced material [123]. This finding was attributed to the difference in the load bearing capabilities and the relative strengths of the two types of reinforcement.

4.4.1. Elevated temperature deformation mechanisms and models

Creep behaviour in particulate reinforced MMCs is characterized by a progressively increasing creep rate (tertiary creep) over most of the creep life. The potential causes of tertiary creep in engineering alloys have recently been reviewed by Dyson and McLean [127] who point to the usefulness of the Monkman–Grant parameter, C_m, and a creep damage factor, η, in identifying the type of damage that causes the accelerating creep. Analysis of the creep curve for Al–SiC_p indicates that $C_m \sim 10^{-2}$ and $\eta \sim 10$ which are far out of range of values for damage mechanisms that lead to tertiary creep and fracture in more conventional metallic alloys, e.g., loss of external section ($C_m \sim 0.2$), and development of creep cavities ($\eta \sim 1$ to 3). More appropriate mechanisms in this case are those dependent on degradation of the microstructure, by thermal coarsening of the particulates or the development of dislocation substructure. The former may be disregarded on account of the relatively low temperatures and high stability of the particulate morphologies. However, the data are similar to those of nickel-base superalloys and Al–Li alloys where tertiary creep has been shown to be a strain softening phenomenon resulting from the progressive accumulation of mobile dislocations [127]. Constitutive equations, based on this physical interpretation, have been developed and expressed, using the formalism of continuum damage mechanics, in terms of two state variables S and ω by Ion *et al.* [108] and Maldini *et al.* [109]

$$\varepsilon = \varepsilon_{min}[(1 - S)/(1 - S_{ss})]exp(\omega) \quad (25)$$

$$S = H\varepsilon_{min}[(1 - S)/(1 - S_{ss}) - S/S_{ss}] \quad (26)$$

$$\omega = H\varepsilon_{min} \quad (27)$$

where S is the ratio of an internal stress caused by local stress distributions and the applied stress that leads to an element of primary creep; ω is a measure of the increase in the density of mobile dislocations ($\rho - \rho_{min}/\rho$), ε_{min} is the minimum creep rate and S_{ss} is the steady state value for S. Strengthening associated with equiaxed particulates is due to the suppression of the natural creep mechanisms that can occur in the monolithic matrix material; e.g., dislocation glide, which occurs readily in the monolithic matrix material, may be prevented by the particulates, thus requiring dislocation motion to occur by slower climb around the particulates.

5. Concluding remarks

The large body of literature reviewed in this paper presents a cross-section of views and experimental results obtained over the years by numerous investigators in the field of particulate reinforced MMCs. Considerable amount of interest in these materials among researchers in both academia and industry led to numerous studies which enriched our understanding of the inter-relationship between processing-microscopic characteristics and macroscopic behaviour.

The results reviewed in this work demonstrate that, although the interface formed between the matrix and the reinforcement has a critical effect on subsequent mechanical behaviour, our current understanding of the interface is limited. For example, direct measurements of the interfacial shear strength in the MMCs have been limited to pull-out tests and punch tests.

Regarding the processing of particulate reinforced MMCs, a variety of techniques have evolved over the past two decades. A critical review of the available literature shows that these processing techniques can be classified according to the temperature of the metallic matrix during processing. Accordingly, liquid phase, solid phase and two phase (solid–liquid) processes are currently available.

Finally, the physical and mechanical properties of particulate reinforced MMCs were also reviewed, with particular emphasis on: strengthening mechanisms, dynamic, static and high temperature behaviour.

Acknowledgements

The authors wish to acknowledge the Army Research Office (grant # DAAL03-89-K-0027), and the National Science Foundation (Grant No. MSS 8957449).

References

1. S. G. FISHMAN, *J. Met.* **38** (1986) 26.
2. Y. FLOM and R. J. ARSENAULT, *ibid.* **38** (1986) 31.
3. *Idem., Mater. Sci. Eng.* **77** (1986) 191.
4. A. H. M. HOWES, *J. Met.* **38** (1986) 28.
5. A. MORTENSEN, M. N. GUNGOR, J. A. CORNIE and M. C. FLEMINGS, *ibid.* **38** (1986) 30.
6. A. MORTENSEN, J. A. CORNIE and M. C. FLEMINGS, *ibid.* **40** (1988) 12.
7. V. C. NARDONE and K. W. PREWO, *Scripta. Metall.* **20** (1986) 43.
8. T. W. CHOU, A. KELLY and A. OKURA, *Composites* **16** (1986) 187.
9. A. P. DIVECHA and S. G. FISHMAN, "Mechanical Properties of Silicon Carbide Reinforced Aluminum, in Proc. 3rd Int. Conf. on Composite Materials, Vol. 3, 1979, 351.
10. A. L. GEIGER and M. JACKSON, *Adv. Mater. Process* **7** (1989) 23.
11. A. K. DHINGRA, *J. Met.* **38** (1986) 17.
12. R. C. FORNEY, *ibid.* **38** (1986) 18.
13. H. J. RACK, in "Processing and Properties of Powder Metallurgy Composites", edited by P. Kumar, K. Vedula and A. Ritter (The Metallurgical Society, Warrendale, PA, 1988) p. 155.
14. S. R. NUTT, *J. Amer. Ceram. Soc.* **67** (1984) 428.
15. A. P. DIVECHA, S. G. FISHMAN and S. D. KARMARKAR, *J. Met.* **33** (1981) 12.
16. R. J. ARSENAULT, *Mater. Sci. Eng.* **64** (1984) 171.
17. C. R. CROWE, R. A. GRAY and D. F. HASSON, in Proceedings of the 5th International Conference in Composite Materials, edited by W. Hanrigaan, J. Strife and A. K. Dhingra (The Metallurgical Society of AIME, Warrendale, PA, 1985) p. 843.
18. S. V. NAIR, J. K. TIEN and R. C. BATES, *Int. Met. Rev.* **30** (1985) 275.
19. A. MORTENSEN, J. A. CORNIE and M. J. C. FLEMINGS, *Met. Trans.* **19A** (1988) 709.
20. M. M. SCHWARTZ, in "Composite Materials Handbook", edited by H. B. Crawford and E. Richardson (McGraw Hill, New York, 1984).
21. Engineering Properties of Selected Ceramic Materials, Battelle Memorial Institute (The American Ceramic Society, Ohio, 1966).
22. H. J. RACK, in Proceedings of the 6th International Conference on Composite Materials, edited by F. L. Matthews, N. C. R. Buskell, J. M. Hodgkinson and J. Morton (Elsevier Applied Science, London, 1987) p. 2.382.
23. T. E. STEELMAN, A. D. BAKALYAR and L. KOROPKA, in "Aluminium Matrix Composite Structural Design Development", AFWAL-TR-86-3087, March 1987.
24. W. H. HUNT, Jr., C. R. COOK, K. P. AMANIE and T. B. GURGANUS, in "Powder Metallurgy Composites", edited by P. Kumar, A. Ritter and K. Vedula (The Metallurgical Society, Warrendale, PA, 1987).
25. W. H. HUNT, Jr., O. RICHMOND and R. D. YOUNG, *ibid.* ref. 3, 2.209.
26. M. E. FINE, in "Dispersion Strengthened Aluminium Alloys", edited by Y. M. Kim and W. Griffith (The Metallurgical Society, Warrendale, PA, 1988) p. 103.
27. G. S. MURTY, M. J. KOCZAK and W. E. FRAZIER, *Scripta Metall.* **21** (1987) 141.
28. W. E. FRAZIER and J. J. THOMPSON, in "Dispersion Strengthened Aluminium Alloys", edited by Y. M. Kim and W. Griffith (The Metallurgical Society, Warrendale, PA, 1988) p. 573.
29. T. G. NIEH, R. A. RAINEN and D. J. CHELLMAN, in Proceedings of the 5th International Conference in Composite Materials, edited by W. Hanrigaan, J. Strife and A. K. Dhingra (The Metallurgical Society of AIME, Warrendale, PA, 1985) p. 825.
30. J. R. CARROL, Jr., in "Dispersion Strengthened Aluminium Alloys", edited by Y.-W. Kim (The Metallurgical Society, Warrendale, PA, 1987).
31. M. RUHLE and A. G. EVANS, *Mater. Res. Symp. Proc.* **120** (1988) 293.
32. R. E. JOHNSON Jr., *J. Phys. Chem.* **63** (1959) 1655.
33. F. DELANEY, L. FROYEN and A. DERUYTTERE, *J. Mater. Sci.* **22** (1987) 1.
34. S. Y. OH, J. A. CORNIE, and K. C. RUSSELL, *Ceramic Engineering Sci. Proc.*, **8** (1987) 912.
35. P. K. ROHATGI, R. ASTHANA and S. DAS, *Int. Met. Rev.* **31** (1986) 115.
36. R. L. MAHAR, R. JAKASAND and C. A. BRUCH, "Behavior Study of Sappire Wool, aluminium and Al alloy composites", Tech. Rep. AFML-TR-68, May 1968.
37. R. L. MEHAN and E. FEINGOLD, *J. Mater.* **2** (1980) 239.
38. H. R. SHELTY and TWU-WEI CHOO, *Met. Trans. A* **16A** (1985) 853.
39. S. M. WOLF, A. P. LEVITT and J. BROWN, *Chem. Eng. Prog.* **62**, 74.
40. A. BANERJEE, MSc Thesis, University of Kerala, India, 1982.
41. C. G. LEVI, G. J. ABASCHIAN and R. MEHRABIAN, *Metall. Trans.* **9A** (1978) 697.
42. M. UEKI, M. KANA and I. OKAMOTO, *J. Mater. Sci. Lett.*, **5** (1986) 1261.
43. DOH-JAE LEE, M. D. VAUDIN, C. A. HANDWERKER and U. R. KATTNER, *Mater. Res. Symp. Proc.* **120** (1988) 293.
44. T. A. CHERNYSHOVA and A. V. REBROV, *J. Less-Common Met.* **117** (1986) 203.
45. W. C. MOSHIE, J. S. AHEARN and D. C. COOKE, *J. Mater. Sci.* **22** (1987) 115.

46. D. J. LLOYD and I. JIN, *Metall. Trans.* **19A** (1988) 3107.
47. R. J. ARSENAULT and C. S. PANDE, *Scripta Metall.* **18** (1984) 1131.
48. L. J. BROUTMAN and R. H. KROCKS, *Compos. Mater.* **1** (1974) 57.
49. A. S. ARGON, J. IM and R. SAFOGLU, *Metall. Trans.* **6A** (1975) 825.
50. A. S. ARGON, J. IM and A. NEEDLEMAN, *ibid.* **6A** (1975) 815.
51. A. S. ARGON and J. IM, *ibid.* **6A** (1975) 839.
52. T. G. NIEH and R. G. KARLAC, *Scripta Metall.* **18** (1984) 25.
53. T. CHRISTMAN and S. SURESH, Brown University Report No. NSF-ENG-8451092/1/87, June 1987.
54. H. J. RACK, in "Dispersion Strengthened Aluminium Alloys", edited by Y. M. Kim and W. Griffith (The Metallurgical Society, Warrendale, PA, 1988).
55. J. M. PAPAZIAN, *Met. Trans.* **19A** (1988) 2945.
56. S. R. NUTT, in "Interfaces in Metal Matrix Composites", edited by A. K. Dhingra and S. G. Fishman (TMS-AIME, Warrendale, PA, 1986) p. 157.
57. S. R. NUTT and R. W. CARPENTER, *Mater. Sci. Eng.* **75** (1985) 169.
58. C. LEA and C. MOLINARI, *J. Mater. Sci.* **19** (1984) 2336.
59. T. MALIS and M. C. CHATURVEDI, *J. Mater. Sci.* **17** (1982) 1479.
60. R. MEHRABIAN, *Mater. Res. Soc. Symp.* **120** (1988) 3.
61. Duralcan Metal Matrix Composites May–June Data Report Package, Dural Aluminium Composites Corporation, San Diego, CA 92121.
62. T. W. CLYNE, M. G. BADER, G. R. CAPPLEMAN and P. A. HUBERT, *J. Mater. Sci.* **20** (1985) 85.
63. T. W. CLYNE and J. F. MASON, *Met. Trans* **18A** (1987) 1519.
64. J. A. CORNIE, A. MORTENSEN and M. C. FLEMINGS, in Proceedings of the 6th International Conference on Composite Materials, ICCM and ECCM, edited by F. L. Matthews, N. C. R. Buskell, J. M. Hodgkinson and J. Morton (Elsevier Applied Science, London, 1987) p. 2.297.
65. T. DONOMOTO, N. MIURAS, K. FUNATANI and N. MIYAKE, SAE Technical Paper no. 83052, Detroit, MI, 1983.
66. B. FERGUSON, A. KUHN, O. D. SMITH and F. HOFSTATIER, *Int. J. Powd. Metall. Powd. Tech.* **20** (1984) 131.
67. M. S. NEWKIRK, A. W. URGUHART, H. R. ZWICKER and E. BREVAL, *J. Mater. Res.* **1** (1986) 81.
68. J. WEINSTEIN, in Proceedings of the International Symposium on Advances in Processing and Characterization of Ceramic Metal Matrix Composites, CIM/ICM, Vol. 17, edited by H. Mostaghaci (Pergamon, Oxford, 1989) p. 132.
69. S. KRISHNAMURTHY, Y-W. KIM, G. DAS and F. H. FROES, in "Metal–Ceramic Matrix Composites: Processing, Modelling and Mechanical Behaviour", edited by R. B. Bhagat, A. H. Claver, P. Kumar and A. M. Ritter (The Minerals, Metals/Materials Society, Warrendale, PA, 1990) p. 145.
70. H. JONES, "Rapid Solidification of Metals and Alloys", Monograph Series no. 8 (The Institute of Metallurgists, 1982).
71. Rapidly Solidified (RS) Aluminium Alloys–Status and Prospects. NMAB-368 (National Academy Press, Washington, D.C. 1981).
72. G. ELKABIR, L. K. RABENBERG, C. PERSAD and H. L. MARCUS, *Scripta Metall.* **20** (1986) 1411.
73. C. PERSAD, S. RAGHNATHAN, B. H. LEE, D. L. BOURELL, Z. ELIEZER and H. L. MARCUS, *Mater. Res. Soc. Symp. Proc.* **120** (1988) 23.
74. T. C. WILLIS, Metals and Materials **4** (1988) 485.
75. J. WHITE, I. G. PALMER, I. R. HUGHES and S. A. COURT, in 'Aluminum-Lithium Alloys V", edited by T. H. Sanders, Jr. and E. A. Starke, Jr. (MCE Publications, Williamsburg, VA 1989) p. 1635.
76. R. MEHRABIAN, R. G. RIEK and M. C. FLEMINGS, *Met. Trans.* **5** (1974) 1899.
77. E. F. FASCETTA, R. G. RIEK, R. MEHRABIAN and M. C. FLEMINGS, *Trans. AFS.* **81** (1973) 81.
78. M. GUPTA, F. A. MOHAMED and E. J. LAVERNIA, *Mater. Manuf. Proc.* **5** (1990) p. 165.
79. *Idem.*, in "Proceedings of the International Symposium on Advances in Processing and Characterization of Ceramic Metal Matrix Composites", CIM/ICM, **17**, edited by H. Mostaghaci (Pergamon Press, Oxford, 1989) p. 236.
80. *Idem.*, in "Heat Transfer Mechanisms and their Effect on Microstructure during Spray Atomization and Co-Deposition of Metal Matrix Composites", edited by S. Fishman, TMS Fall Meeting, Detroit, MI (1990).
81. P. S. TURNER, *J. Res. NBS*, **37** (1946) 239.
82. E. H. KENER, *Proc. Phys. Soc.* **68B** (1956) 808.
83. L. RALEIGH, *Phil. Mag.* **34** (1982) 481.
84. J. HASHIM and S. SHTRIKMAN, *J. Mech. Phys. Solids* **11** (1963) 127.
85. D. L. McDANELS, *Met. Trans. A.* **16A** (1985) 1105.
86. R. J. ARSENAULT and R. M. FISHER, *Scr. Metall.* **17** (1983) 67.
87. M. F. ASHBY, *Phil. Mag.* **21** (1970) 399.
88. M. VOGELSANG, R. J. ARSENAULT and R. M. FISHER, *Metall. Trans.* **17A** (1986) 379.
89. J. K. LEE, Y. Y. EARMME, H. I. AARONSON and K. C. RUSSELL, *Met. Trans.* **11A** (1980) 1837.
90. G. S. ANSELL, in "Oxide Dispersion Strengthening", edited by G. S. Ansell, T. D. Cooper and F. V. Lenel (Gordon and Breach, New York, 1968), p. 61.
91. E. OROWAN, in "Symposium on Internal Stresses in Metals and Alloys" (Institute of Metals, Ohio, 1948), p. 451.
92. M. F. ASHBY, *Z. Metallk.* **55** (1964) 5.
93. P. GUYOT, in "1965 International Powder Metallurgy Conference" (Plenum, New York, 1966).
94. J. FRIEDEL, in "Dislocations" (Addison-Wesley, Reading, Mass, 1964).
95. D. DEW-HUGHES, *Acta Metall.* **8** (1960) 816.
96. J. C. FISHER, E. W. HART and R. H. PRY, *ibid.* **1** (1953) 336.
97. G. S. ANSELL and F. V. LENEL, *ibid.* **8** (1960) 612.
98. A. KELLY and R. B. NICHOLSON, "Progress in Materials Science", Vol. 10, No. 3 (Macmillan, New York, 1969).
99. G. S. ANSELL, *Acta Metall.* **9** (1961) 518.
100. J. D. ESHELBY, *Proc. Roy. Soc.* **A241** (1957) 376.
101. T. MURA and M. TAYA, in Proceedings of the 2nd U.S.-Japan Conference on Comp. Mat. ASTM, under review.
102. K. TANAKA and T. MORI, *Acta Metall.* **18** (1970) 931.
103. R. J. ARSENAULT and M. TAYA, *ibid.* **35** (1987) 651.
104. R. J. ARONE, O. BOTSTEIN and B. SHIPIGLERF, *Israel J. Tech.* **24** (1988) 393.
105. Y. FLOM and R. J. ARSENAULT, in Proceedings of 6th ICCM—2nd ECCM Congress on Composite Materials, edited by F. L. Matthews *et al.*, 20–24 July 1987, London, UK, 2.189.
106. S. S. YAM and MAYER, *Mater. Sci. Eng.* **82** (1986) 45.
107. J. L. WALTER, in "In-situ Composites IV", edited by F. L. Lemkey *et al* (Elsevier–North Holland, Amsterdam, 1984).
108. J. C. ION, A. BALBOSA, M. F. ASHBY, B. F. DYSON and M. MCLEAN, NPL report No. DMA(A) 115, National Physical Laboratory, April 1986.
109. M. MALDINI, A. BALBOSA, M. F. ASHBY, B. F. DYSON and M. MCLEAN, NPL Report No. DMA(A) 126, National Physical Laboratory, January 1987.
110. B. D. MARSHALL, B. N. COX and A. G. EVANS, *Acta Metall.* **33** (1985) 2013.
111. L. N. MacCARTNEY, *Proc. Roy. Soc.* **A409** (1987) 329.
112. B. BUDIANSKY, in Proceedings of the 10th US Congress Applied Mechanics, Austin, TX, 1986.
113. S. KUNZ-DOUGLASS, P. W. R. BEAUMONT and M. F. ASHBY, *J. Mater. Sci.* **15** (1980) 1109.
114. Y. MAI and B. R. LAWN, *J. Amer. Ceram. Soc.* **70** (1987) 289.
115. W. W. GERBERICH, in "Fracture: Interactions of Microstructure, Mechanisms and Mechanics", edited by J. M. Wells and J. D. Landes (TMS-AIME, Warrendale, PA, 1984) p. 49.
116. A. R. ROSENFIELD and B. S. MAJUNDAR, *Metall. Trans.* **18A** (1987) 1053.

117. J. K. SHANG and R. O. RITCHIE, *Met. Trans. A.* **20** (1989) 897.
118. R. MARISSEN, in "Fatigue 87, Proc. Third International Conference on Fatigue", edited by R. O. Ritchie and E. A. Starke (EMAS Ltd., 1988) vol. 3, p. 1271.
119. J. K. SHANG, W. YU and R. O. RITCHIE, "Role of the Silicon Carbide Particles in Fatigue of Silicon Carbide Particulate-Reinforced Aluminium Alloy Composites", Report No. UCB/R/87/A1048, University of California, Berkeley.
120. J. K. SHANG and R. O. RITCHIE, *Met. Res. Soc. Proc.* **1320** (1988) 81.
121. J. K. SHANG, W. YU and R. O. RITCHIE, *Mat. Sci. Eng.* **102** (1988) 181.
122. M. MCLEAN, *Mater. Res. Soc. Proc.* **120** (1988) 67.
123. T. G. NIEH, *Metall. Trans* **15A** (1984) 139.
124. V. C. NARDONE and J. R. STRIFE, *ibid.* **18A** (1987) 109.
125. T. G. NIEH, K. XIA and T. G. LANGDON, *J. Eng. Mats. Tech.* V **110** (1988) 77.
126. K. PARK, F. MOHAMED and E. LAVERNIA, *Israel J. Tech.* **24** (1988) 369.
127. B. F. DYSON and M. MCLEAN, *Acta Metall.* **17** (1983) 17.

Received 20 November
and accepted 1 December 1989